Succination is Increased on Select Proteins in the Brainstem of the NADH dehydrogenase (ubiquinone) Fe-S protein 4 (Ndufs4) Knockout Mouse, a Model of Leigh Syndrome*[S]

Gerardo G. Piroli‡, Allison M. Manuel‡, Anna C. Clapper‡, Michael D. Walla§, John E. Baatz¶, Richard D. Palmiter‖, Albert Quintana‖**, and Norma Frizzell‡ ‡‡

Elevated fumarate concentrations as a result of Krebs cycle inhibition lead to increases in protein succination, an irreversible post-translational modification that occurs when fumarate reacts with cysteine residues to generate S-(2-succino)cysteine (2SC). Metabolic events that reduce NADH re-oxidation can block Krebs cycle activity; therefore we hypothesized that oxidative phosphorylation deficiencies, such as those observed in some mitochondrial diseases, would also lead to increased protein succination. Using the Ndufs4 knockout (Ndufs4 KO) mouse, a model of Leigh syndrome, we demonstrate for the first time that protein succination is increased in the brainstem (BS), particularly in the vestibular nucleus. Importantly, the brainstem is the most affected region exhibiting neurodegeneration and astrocyte and microglial proliferation, and these mice typically die of respiratory failure attributed to vestibular nucleus pathology. In contrast, no increases in protein succination were observed in the skeletal muscle, corresponding with the lack of muscle pathology observed in this model. 2D SDS-PAGE followed by immunoblotting for succinated proteins and MS/MS analysis of BS proteins allowed us to identify the voltage-dependent anion channels 1 and 2 as specific targets of succination in the Ndufs4 knockout. Using targeted mass spectrometry, Cys[77] and Cys[48] were identified as endogenous sites of succination in voltage-dependent anion channels 2. Given the important role of voltage-dependent anion channels isoforms in the exchange of ADP/ATP between the cytosol and the mitochondria, and the already decreased capacity for ATP synthesis in the Ndufs4 KO mice, we propose that the increased protein succination observed in the BS of these animals would further decrease the already compromised mitochondrial function. These data suggest that fumarate is a novel biochemical link that may contribute to the progression of the neuropathology in this mitochondrial disease model. *Molecular & Cellular Proteomics 15: 10.1074/mcp.M115.051516, 445–461, 2016.*

We previously identified the formation of S-(2-succino)cysteine (2SC)[1] (protein *succination*) as a result of the irreversible reaction of fumarate with reactive cysteine thiols (1, 2). Fumarate concentrations are increased during adipogenesis and adipocyte maturation (2, 3), and the excess of glucose and insulin leads to augmented protein succination in the adipose tissue of type 2 diabetic mice (4, 5). Protein succination is also specifically increased in fumarate hydratase deficient hereditary leiomyomatosis and renal cell carcinoma (HLRCC), because of the decreased conversion of fumarate to malate (6, 7). In both cases, intracellular fumarate concentrations are elevated; in fumarate hydratase deficient cells, the fumarate concentration is about 5 mM (8), whereas fumarate levels

[1] The abbreviations used are: 2SC, S-(2-succino)cysteine; 2D, two-dimensional; BS, brainstem; CB, cerebellum; C[PE], cysteine pyridylethylation; Crus 1, crus 1 ansiform lobule; C[2SC], cysteine succination by fumarate; Ctx, cortex; ER, endoplasmic reticulum; FN, fastigial nucleus; GC, gas chromatography; Gi, gigantocellular reticular nucleus; GSH, glutathione; HLRCC, hereditary leiomyomatosis and renal cell carcinoma; HNE, 4-hydroxy-2-nonenal; IO, inferior olive; MD, mitochondrial diseases; M[OX], methionine oxidation; Mt, microtubular pellet; OB, olfactory bulb; OXPHOS, oxidative phosphorylation; PVDF, polyvinylidene difluoride; RIPA, radioimmuno precipitation assay; SMt, supernatant after tubulin polymerization; SN, sciatic nerve; Str, striatum; Sup, cleared supernatant; VDAC, voltage-dependent anion channel; VN, vestibular nuclei.

increase up to fivefold in adipocytes grown in the presence of high (30 mM) *versus* normal (5 mM) glucose concentrations (2). In the adipocyte the increase in fumarate and succinated proteins develops as a direct result of mitochondrial stress induced by nutrient excess. Mechanistically, excess glucose without increased ATP demand inhibits the electron transport chain resulting in an elevated NADH/NAD$^+$ ratio. This inhibits NAD$^+$-dependent Krebs cycle enzymes and leads to an increase in fumarate and protein succination (9). In support of this we have also shown that low concentrations of chemical uncouplers of oxidative phosphorylation (OXPHOS) can decrease fumarate concentrations and protein succination (9). The physiological consequences of protein succination include a decrease in the functionality of the target protein (8, 10–12), for example succination of adiponectin prevents the formation of multimeric complexes and reduces plasma adiponectin levels in diabetes (4). Considering the impact of glucotoxicity driven mitochondrial stress in the adipocyte, we predicted that deficiencies in OXPHOS associated with NADH accumulation would also result in increased protein succination.

Mitochondrial respiratory chain disorders encompass a broad range of encephalopathies and myopathies associated with the defective assembly, activity or maintenance of the OXPHOS machinery (13), and are estimated to occur in about 1 in 5,000 live births (14). A common feature in most mitochondrial diseases (MD) is a failure to thrive because of reduced mitochondrial energy production; both the brain and muscle are usually affected because of their high dependence on oxidative metabolism (13). Leigh syndrome is one of the most common manifestations of MD and is characterized by progressive neurodegeneration with bilateral necrotizing lesions of the brainstem and basal ganglia, resulting in lactic acidosis, ataxia, seizures, dystonia, and respiratory failure (15, 16). Mutations in genes encoding the five complexes of the OXPHOS machinery can lead to Leigh syndrome; however, the majority of these mutations affect subunits of complexes I and IV (17), and both mitochondrial and nuclear encoded proteins may be affected (17–19). Complex I is a large (980 kDa) L-shaped protein assembly consisting of 45 peptides, with one flavin mononucleotide and eight iron–sulfur clusters (20). One of the first identified mutations of complex I encoded Ndufs4, a small (18 kDa) assembly protein (21–23). Ndufs4 assists in the final stages of complex I assembly, and its absence results in the formation of a smaller ~830 kDa subcomplex that lacks the NADH dehydrogenase module and has significantly less electron shuttling activity than the intact holoenzyme (24, 25). *Ndufs4* mutations are associated with brainstem deterioration in humans (26), and a recently described Ndufs4 knockout mouse (Ndufs4 KO) exhibits many of the clinical and neurological symptoms observed in human Leigh syndrome (27, 28).

One of the most common clinical features of MD is lactic acidosis, derived from the accumulation of pyruvate and elevated NADH. Increased lactate or lactate:pyruvate ratios have been measured in the blood, urine, and cerebrospinal fluid of a large number of Leigh syndrome patients (15, 16). Increases in other organic acids in urine have also been reported (16), indicating that metabolic acidosis is a prominent clinical feature. Interestingly, a study designed to find new diagnostic metabolites in MD demonstrated that within certain age ranges the measurement of urinary fumarate and malate was a more useful discriminator of MD than lactate or other organic acids (29). Barshop's findings support the hypothesis that MD derived from OXPHOS deficiencies may exhibit increased protein succination because of the accumulation of NADH and subsequently fumarate. In this study we report for the first time that protein succination is present in the brain in an animal model of Leigh syndrome, the Ndufs4 KO mouse, suggesting that this modification may be an important biochemical link between the genetic defect and the onset of neuropathology observed in Leigh syndrome.

EXPERIMENTAL PROCEDURES

Chemicals—Unless otherwise noted, all chemicals were purchased from Sigma/Aldrich Chemical Co (St. Louis, MO). Criterion polyacrylamide gels, nitrocellulose membranes and Precision Plus protein ladder were purchased from BioRad Laboratories (Richmond, CA). Polyvinylidene difluoride (PVDF) membranes and ECL Plus chemiluminescent substrate were from GE Healthcare (Piscataway, NJ). The preparation of the polyclonal anti-2SC antibody has been described previously (2). The following commercial antibodies were used: α-tubulin DM1A, VDAC2 9412 from Cell Signaling Technology, Inc. (Danvers, MA); β-tubulin TUB2.1 from Santa Cruz Biotechnology (Dallas, TX); HNE (HNE-11-S) from Alpha Diagnostics International, Inc. (San Antonio, TX); Ndufs4 2C7CD4AG3 and DJ1 ab4150 from Abcam (Cambridge, MA); VDAC1 clone N152B/23 from Antibodies Inc. (Davis, CA), and glutathione from Virogen Corporation (Watertown, MA).

Animals and Tissue Preparation for Protein Analysis—Animal care and use procedures were carried out in accordance with protocols written under the guidelines of the National Institutes of Health Guide for the Care and Use of Laboratory Animals and approved by The University of South Carolina Animal Care and Use Committee. Ndufs4 heterozygous mice were obtained from Drs. Richard Palmiter and Albert Quintana (Seattle Children's Research institute, Seattle, WA). After 2 weeks of acclimatization to the University of South Carolina School of Medicine Animal Facility, breeding pairs were mated, and the litters were weaned at 21 days of age. Genotyping was performed as previously described (28). KO and WT mice were sacrificed by CO_2 asphyxiation at early (3 weeks), middle (6 weeks), and late (9 weeks) stages, and brain, sciatic nerves and skeletal muscle were removed immediately; tissues with the exception of the brain (see below) were snap frozen in liquid nitrogen and stored at $-80\ °C$ until further use. Some brains were subjected to macro dissection before freezing; isolated regions included the brainstem (BS), cerebellum (CB), cerebral cortex (Ctx), striatum (Str), and olfactory bulb (OB). For the microdissection of CB and BS areas, the posterior half of the brain was frozen and sliced at 400 μm in a cryostat (Microm HM 560) between Bregma -5.40 and -7.00 mm, according to a mouse brain atlas (30). Brain slices were mounted on microscope glass slides, and the vestibular Nuclei (VN), inferior olive/gigantocellular reticular nuclei (IO/Gi), fastigial nuclei (FN), and crus 1 ansiform lobule (Crus 1) were punched out of the slices using a Harvard Apparatus puncher (1.0 mm diameter); all punches from the same region were collected in one tube per mouse.

Radioimmunoprecipitation assay (RIPA) lysis buffer (50 mM Tris-HCl, 150 mM NaCl, 1 mM EDTA, 0.1% Triton X-100, 0.1% SDS, 0.5% sodium deoxycholate, pH 7.4), with the addition of 2 mM diethylene-triaminepentaacetic acid and a protease inhibitor mixture (P8340, Sigma/Aldrich) was added to tissues that were used for gel separation procedures. Homogenization was performed by pulse sonication at 2 watts using a Model 100 sonic dismembrator (Fisher Scientific, Fair Lawn, NJ) for 30 s prior to resting on ice for 30 min in lysis buffer. The homogenate was clarified from nuclei and unbroken cells by centrifugation at $900 \times g$ for 10 min at 4 °C. Protein in the supernatants was precipitated with 9 volumes of cold acetone for 10 min on ice. After centrifugation at $3000 \times g$ for 10 min and removal of the acetone, the protein pellet was resuspended in 500 μl RIPA buffer. For the identification of succination sites in VDAC2 (see "Identification of Succinated Cysteines in Tubulin and VDAC2 by LC-MS/MS" below), subcellular fractions were prepared from WT Ctx and from WT and Ndufs4 KO BS , according to Frezza et al. (31). Briefly, tissues were homogenized in 10 mM Tris-HCl (pH 7.4), 1 mM EGTA, 200 mM sucrose, and a protease inhibitor mixture (P8340, Sigma/Aldrich), using a Teflon pestle operated homogenizer. The homogenate was cleared of cell nuclei and unbroken cells by centrifugation at $600 \times g$ for 10 min at 4 °C; the supernatant was further centrifuged at $7000 \times g$ for 10 min at 4 °C. The second supernatant was considered the cytosolic fraction and the pellet containing the mitochondria was resuspended in homogenization buffer. Analysis by Western blotting of the initial homogenate, cytosol and mitochondrial fractions showed an enrichment of mitochondrial markers in the mitochondrial fraction (citrate synthase); tubulin was found concentrated in the cytosolic fraction (data not shown). The protein content in the different samples was determined by the Lowry assay (32).

Lentiviral Transduction of N1E-115 Cells—Vector Preparation: The lentiviral vectors were prepared by the University of South Carolina Viral Vector Facility. Briefly, TRC2 Fh1 shRNA, clone-TRCN0000246831 or SHC202 MISSION TRC2 pLKO.5-puro Non-Mammalian shRNA control plasmids (Sigma/Aldrich) were used to generate the lentiviral vectors. The vectors also contained a puromycin resistance gene. 15 μg vector plasmid, 10 μg psPAX2 packaging plasmid (Addgene 12260, Cambridge, MA), 5 μg pMD2.G envelope plasmid (Addgene 12259) and 2.5 μg pRSV-Rev plasmid (Addgene 12253) were transfected into 293T cells. The filtered conditioned medium was collected and stored at −80 °C until use.

N1E-115 cells (subclone N1E-115–1 neuroblastoma cells) were obtained from Sigma (08062511). The cells were grown in non-differentiation medium (NDM, 90% DMEM (Gibco, Grand Island, NY) with 25 mM glucose, no pyruvate, 25 mM HEPES, 4 mM Glutamine) and 10% Fetal Bovine Serum (Atlanta Biologicals, Atlanta, GA) in 25 cm^2 flasks.

At 80% confluence, the cells in 25 cm^2 were washed with Dulbecco's PBS and 1.5 ml NDM was added prior to addition of 300 μl of lentiviral vector conditioned medium for cell transduction.

The cells were incubated for 18 h before returning the volume to 4.5 ml with NDM. After 48 h selection of transduced cells with puromycin (1.75 μg/ml, determined by a dose response curve, Sigma/Aldrich) was initiated for 1 week. At the end of this period, the remaining cells were expanded and differentiated into neurons in the presence of 2% FBS, 1.25% DMSO in DMEM in addition to 1 μg/ml puromycin for 5 days. The cells were harvested in RIPA as described previously (12) and the levels of fumarase (to assess efficiency of shRNA knockdown) and protein succination were determined by immunoblotting (described below). In a separate experiment the levels of fumarate were determined by GC-MS (described below).

Quantification of Fumarate in N1E-115 Neurons—The quantification of fumarate was performed by GC-MS at the David H. Murdock Research Institute (DHMRI, Kannapolis, NC). Metabolite extraction was performed in an adaptation of previous methods (9). Briefly, N1E-115 cells grown in 25 cm^2 flasks were washed three times with ice-cold PBS followed by the immediate addition of 20 volumes ice-cold chloroform/methanol (2:1). The samples were vortexed and allowed to stand on ice for 10 min with intermittent vortexing prior to addition of 0.2 volumes H$_2$O. The samples were vortexed and allowed to stand on ice for an additional 2 min, followed by centrifugation at $3220 \times g$ for 20 min. The aqueous supernatant was transferred into a clean tube and dried under air. The extraction was repeated an additional time by adding equal parts of methanol and deionized water, centrifuging, and transferring the aqueous layer into the respective tube to dry. The protein interface for each sample was removed for quantification of protein by Lowry assay (32). Prior to derivatization the extracts were resuspended in ethyl acetate and transferred to GC-MS vials. The samples were dried with N$_2$, and an internal standard (100 μM succinate-$^{13}C_4$, Cambridge Isotope Laboratories, Inc. Tewksbury, MA) was added to each of the samples and fumarate standards. The samples and standards were derivatized with 200 μl of methylamine (20 mg/ml in pyridine, M.P. Biomedicals, Solon, OH) at 30 °C for 90 min, followed by drying under N$_2$. This was followed by the addition of 120 μl of N-methyl-N-(trimethylsilyl) trifluoroacetamide (MSTFA, Sigma) with 1% trimethylchlorosilane (TMCS, Sigma); the mixture was incubated at 70 °C for 60 min. The derivatized product was stored in a −20 °C freezer for one hour. A 100 μl aliquot of the prepared product was transferred to a deactivated glass insert in a 2 ml glass vial (Agilent Technologies, Santa Clara, CA) for GC/MS analysis.

An Agilent 7890A GC system, coupled to an Agilent 5975C electron ionization (EI) mass selective detector (MSD) was used to analyze the TMS-derivatized samples. A column with dimensions 30 m $\times$ 0.25 mm I.D ., 0.25 μm film thickness (Restek, Bellefonte, PA) was used, and the column operation conditions were as follows: helium carrier gas at 1.0 ml/min; GC oven temperature program of 70 °C (2 min), 70–100 °C (30 °C/min, 1 min), 100–140 °C (10 °C/min, 4 min), 140–188 °C (4 °C/min, 12 min), 188–280 °C (5 min), with a transfer line temperature of 270 °C. The GC-MS was operated under a splitless mode (inlet at 250 °C). The mass spectrometry was performed at an electron energy of −70 eV and the ion source temperature was 230 °C. Selected ion monitoring (SIM) was performed for fumarate and the peak areas obtained were normalized to the added internal standard. Absolute quantitation was performed based on standard curves obtained from the normalized reference standards, and the final metabolite concentrations were normalized to the protein content of the cells.

One-dimensional PAGE and Western Blotting—Western blotting to probe for protein succination (2SC), Ndufs4, HNE, VDAC1, VDAC2, and tubulin was performed as described previously, after separation of the proteins by SDS-PAGE (2, 12). For glutathione (GSH)-modified proteins, reducing agents were omitted during sample preparation and gel electrophoresis. Some gels were stained with Coomassie brilliant blue for band isolation and mass spectrometry (see below). In some cases, membranes were stripped with 62.5 mM Tris, pH 6.8, containing 2% SDS and 0.7% 2-mercapto ethanol for 20 min at 65 °C prior to reprobing with a different antibody.

Two-dimensional Gel Electrophoresis—Isoelectric focusing on pI 4–7 11 cm strips and two-dimensional (2D) gel electrophoresis was performed as described previously (2, 12). The 2D gels were stained for protein using Coomassie brilliant blue (ProtoSafe Blue; National Diagnostics, Atlanta, GA) or transferred onto PVDF membranes to detect protein succination, VDAC1, VDAC2, DJ-1 and tubulin by Western blotting. Images of the stained gels and chemiluminescent blots were acquired at 200 micron resolution using a Typhoon Trio+ Imager using appropriate filters. Image overlay, spot detection, alignment and analysis were performed using SameSpots (Nonlinear Dy-

namics Durham, NC) 2D analysis software (v 4.2). Spot picking was performed using an Amersham Biosciences/GE Healthcare Ettan SpotPicker (4).

Protein Identification from 2D Gel Spots by LC-MS/MS—The gel digestion methods used were previously described (2, 33). Briefly, spots of interest were excised from gels after staining with Coomassie Brilliant Blue. The gel spots were washed with 50 mM ammonium bicarbonate in 50% acetonitrile, followed by dehydration with 100% acetonitrile; proteins were then reduced with 10 mM dithiothreitol and alkylated with 100 mM iodoacetamide. Trypsin digestion was carried out overnight at 37 °C in the presence of 1.5 ng sequence grade modified trypsin (Promega, Madison, WI) in 50 mM ammonium bicarbonate. The supernatant and extracts with 5% formic acid in 50% acetonitrile, and 100% acetonitrile were pooled and dried down in a SpeedVac centrifuge to ~2 μl. Prior to LC-MS/MS analysis the samples were reconstituted with 7 μl of 2% acetonitrile and 0.2% formic acid. LC was performed using a 75 μm × 20 cm fused-silica column packed in house with C18 reversed-phase resin (YMC-ODS-AQ; 5-μm particles; 200-Å pore; Waters, Milford, MA) with a 120 min gradient from 5% acetonitrile, 0.2% formic acid to 50% acetonitrile, 0.2% formic acid on a LC Packings U3000 nano LC system at a flow rate of 200 nl/min. The sample was introduced via nano-electrospray ionization (nESI) to a hybrid dual-pressure linear ion trap-orbitrap mass spectrometer (Orbitrap Elite, Thermo Fisher Scientific , Rockford, IL). Mass spectra were acquired in data dependent mode using a TOP20 method which acquires one FTMS survey MS scan in the mass range of m/z 400–2000 followed by tandem mass spectra (MS/MS) of the twenty most intense ions in the LTQ Velos. The automatic gain control target value in the Orbitrap was 10^6 for the survey MS scan at a resolution of 60,000 at m/z 400. A lock-mass was used to compensate for calibration drift. Fragmentation in the LTQ was performed by collision induced dissociation with a target value of 10000 ions and a threshold of 500 counts. The raw data were searched with the Sequest HT node of Proteome Discoverer 1.4 (SP1). The uniprot_ref_mouse database (55,250 protein entries), downloaded September 2012, was utilized for the searches. Variable modifications of methionine oxidation and succinated cysteines were considered. All protein identification results were filtered to include only high confidence peptides with an Xcorr *versus* charge state > 1.5, 2.0, 2.5 for +1, +2, and +3 ions, peptide mass deviation < 10ppm, charge state >2, and a minimum of 2 unique peptides per protein. The mass tolerance of fragment ions was <0.8 Da.

Identification of Succinated Cysteines in Tubulin and VDAC2 by LC-MS/MS—For the identification of succination sites in tubulin, microtubules were obtained from Ndufs4 KO mice BS as described below (see "Purification and Polymerization of Mouse Brain Tubulin"). For the identification of succination sites in VDAC2, we first used mitochondrial fractions from mouse brain Ctx that were incubated in 100 mM fumarate for 18 h at 37 °C, we then investigated the sites of endogenous succination of VDAC2 from BS mitochondrial fractions of Ndufs4 KO mice. In all cases, samples were resolved by SDS-PAGE, and the gels were stained with Coomassie Brilliant blue. After destaining, the corresponding bands (tubulin at ~50–55 kDa; VDAC1 and 2 at ~30–35 kDa) were excised from the gels and subjected to in gel digestion with trypsin as described above (see "Protein Identification by LC-MS/MS"), with the exception of alkylation with 170 mM 4-vinylpyridine. After gel extraction, the digested samples were resuspended in 1% acetic acid and analyzed on a Dionex Ultimate 3000-LC system (Thermo Scientific) coupled to a Velos Pro Orbitrap mass spectrometer (Thermo Scientific). The LC solvents were 2% acetonitrile/0.1% formic acid (Solvent A) and 80% acetonitrile/0.1% formic acid (Solvent B). At 4 min the trap column, a 2 cm Acclaim PepMap-100 column (Thermo Scientific) was put in line with the analytical column, a 75 μm C18 stationary-phase LC PicoChip Nano-

spray column (New Objective, Inc., Woburn, MA). The peptides were eluted with a gradient from 98%A/2%B to 40%A/60%B over 30 min, followed by a 5 min ramp to 10%A/90%B that was held for 10 min. The Orbitrap was operated in data-dependent MS/MS analysis mode and excluded all ions below 200 counts. An inclusion list of up to 8 abundant isotopic masses ± 3 amu was used to confirm protein identity. To further identify specific succinated sites MRM was used to monitor select pyridylethylated and succinated tryptic peptide masses of interest (generated using ProteinProspector, v 5.14.1) for CID (collision-induced dissociation)-MS/MS analysis at a resolution of 7500. The data-dependent and CID-MS/MS data were analyzed using Proteome Discover 1.4 software with SEQUEST search engine against the uniprot_ref_mouse database (2014–10–03 version, 52,474 proteins) with Xcorr >2 validation (+2) and allowance for 1 missed cleavage. The CID-MS/MS data was sequenced manually using Thermo Xcalibur 2.2 software to confirm the modified peptides. The variable modifications of methionine oxidation (M^{OX}), cysteine pyridylethylation (C^{PE}, 105.058) or cysteine succination (C^{2SC}) by fumarate (116.011) were considered with a mass tolerance of 15 ppm for precursor ions and a mass tolerance of 10 ppm for fragment ions. The mass spectrometry proteomics data have been deposited to the ProteomeXchange Consortium via the PRIDE partner repository with the data set identifier PXD002991 and 10.6019/PXD002991.

Quantification of 2SC by Gas Chromatography-Mass Spectrometry (GC-MS/MS)—The procedure was adapted from previously described methods with minor modifications (1, 2, 12). BS, CB, Ctx, OB, muscle and microtubular fractions (see Purification and Polymerization of Mouse Brain Tubulin below) proteins were precipitated by addition of an equal volume of cold 20% trichloroacetic acid, followed by centrifugation at 1000 × g for 10 min at 4 °C. Pellets were hydrolyzed in 6 M HCl containing 0.5 nmol $^{13}C_3,^{15}N$-2SC, and 100 nmol d_8-lysine internal standards for 16 h at 110 °C. The dried sample was resuspended in 1 ml 1% trifluoroacetic acid (TFA) and applied to a C-18 Sep-Pak column (Waters) before elution with 1% TFA/20% methanol. The eluate was dried *in vacuo* and the residual amino acids were converted to their *N,O*-trifluoroacetyl methyl ester (TFAME) derivatives for GC-MS/MS analysis as previously described (1, 2, 12). Quantification was performed by isotope-dilution mass spectrometry based on standard curves. The 2SC content was normalized to the lysine content of the samples, as this correlates with the total protein content.

Purification and Polymerization of Mouse Brain Tubulin—In vitro polymerization of mouse brain tubulin was performed according to a previously described protocol (34), with minor modifications (12). Briefly, frozen BS from WT and Ndufs4 KO mice were reduced to a powder with a pestle in a mortar containing liquid nitrogen. The pulverized brains were then resuspended in cold Mes/glutamate buffer (0.1 M Mes, pH 6.8, containing 0.5 mM MgCl₂, 1 mM EGTA, 1 M glutamate, 1 mM DTT, and a protease inhibitor mixture), in a volume ratio of 1:1.5 (powder/buffer). The suspension was pulse sonicated at 2 watts using a Model 100 sonic dismembrator (Fisher Scientific) for five intervals of 10 s. The total protein homogenate was then centrifuged at 30,000 × g at 4 °C for 15 min to remove cell debris, and the cleared supernatant (Sup) was subjected to polymerization by addition of 20 μM taxol and 1 mM GTP, followed by incubation for 30 min at 37 °C. Following further centrifugation at 30,000 × g for 30 min at 37 °C, the supernatant of microtubules (SMt) was removed and collected, and the microtubular pellet was washed by resuspension with Mes/glutamate buffer containing 0.35 M NaCl and 20 μM taxol, to remove loosely bound proteins. A purified microtubular pellet (Mt) was obtained by centrifugation at 30,000 × g for 30 min at 37 °C. The Mt fractions were re-suspended in a mix of 50% RIPA buffer/50% PBS. All the fractions were kept at −70 °C until use. Protein loading

from each fraction for SDS-PAGE was performed on a volume basis using the equivalent of 1 μg protein from the Sup fraction.

Experimental Design and Statistical Analysis—Analyses were performed with a minimum of three independent biological replicates per group ($n = 3$). Data are summarized throughout as means $\pm$ S.E. and are plotted using SigmaPlot 11 software (Systat Software, Inc. San Jose, CA) and Prism 4 (GraphPad Software, La Jolla, CA). Statistical analyses were performed using SigmaPlot 11 and Prism 4. When two groups were compared, the Student "t" test was used. Differences between more than 2 groups were analyzed using one way ANOVA with the Student-Newman-Keuls post-test. In all cases, $p < 0.05$ was considered statistically significant.

RESULTS

The Ndufs4 KO mice in this study displayed the characteristic features previously reported in this model of Leigh syndrome, including decreased motor activity and the loss and regain of hair (27). Body weight was significantly different from WT littermates from 4 weeks of age until sacrifice (supplemental Fig. S1A). We also confirmed that the Ndufs4 subunit of the electron transport chain Complex I was absent in the brainstem (BS) of KO mice (supplemental Fig. S1B). To determine if the OXPHOS deficiency was associated with fumarate accumulation and protein succination, we examined 2SC levels in several brain regions and the muscle from early (3 weeks), middle (6 weeks) and late (9 weeks) disease stage KO mice and their corresponding WT littermate controls. As shown in Fig. 1A (2SC panel), protein succination in the BS of the KO mice was clearly increased compared with age-matched WT mice as detected by the anti-2SC antibody. Increased succination in the BS of KO mice was especially prominent for proteins of ~25–35 and ~70–80 kDa. An intensely succinated band at ~50–55 kDa was observed in all samples, even in early WT mice, and the intensity of this band initially appeared to increase in the KO BS in association with progressive disease severity. This abundant succinated protein was suspected to be tubulin, and this was subsequently confirmed by LC-MS/MS (Fig. 2). In contrast, only one major band (also at ~50–55 kDa) was detected with the anti-2SC antibody in the muscle of all mice, with no increases because of age or genotype (Fig. 1B, 2SC panel). Interestingly, although actin (A, Fig. 1B, Coomassie panel) is much more abundant in muscle, tubulin (T, Fig. 1B, 2SC panel) is the primary succinated protein, confirming the selectivity of the modification for certain proteins (12).

Increased protein modification by the reactive lipid peroxidation product 4-hydroxy-2-nonenal (HNE) has been described in neurodegenerative diseases (35–37). Several mitochondrial enzymes, including the pyruvate dehydrogenase, α-ketoglutarate dehydrogenase and branched-chain α-keto acid dehydrogenase complexes are targets of HNE conjugation (38). We therefore studied the HNE modification of proteins in the BS of WT and Ndufs4 KO mice, and, although HNE-modified proteins were detected, we did not observe significant changes associated with the genotype or age of the mice (Fig. 1C, HNE panel). Protein oxidation has also been

described in the BS of Ndufs4 KO mice (28), and reduced glutathione levels are lower in lymphocytes and whole blood (39, 40), as well as in muscle of mitochondrial disease patients (41). We also studied protein glutathionylation in our samples, as this is a mechanism that protects sensitive sulfhydryl groups from irreversible oxidation (42). We did not detect any changes in the glutathionylation status of proteins in the BS of Ndufs4 KO mice *versus* age-matched controls (Fig. 1D, GSH panel).

The BS is one of the most affected regions of the Ndufs4 KO mouse brain in terms of the morphological changes associated with pathology, but the olfactory bulb (OB) and the cerebellum (CB) also display some pathology; whereas other areas such as the cortex (Ctx) and striatum (Str) do not appear to be morphologically altered (28). We extended our analysis of succination to the above-mentioned areas in the brains of late stage mice. Basal succination was present in all brain regions of WT mice, with tubulin succination (~50 kDa) apparent in all regions. In contrast, there were more prominent increases in succination on several select proteins in the areas with major morphological changes in the KO mice, namely the OB, CB, and BS (supplemental Fig. S1C). An equivalent amount of muscle protein showed no detectable protein succination in either WT or KO mice at this exposure (supplemental Fig. S1C), confirming our observations that alterations in protein succination are associated with the sites of pathology in this model of MD. We also studied succination in the sciatic nerve (SN), a tissue that contains more stable microtubules bearing a lower level of basal succination than the BS in healthy control mice (12). Our results show that protein succination remained unchanged in the SN of Ndufs4 KO mice compared with WT animals (supplemental Fig. S1D, left panel). When an approximately equal amount of tubulin was compared for the BS (5 μg total protein) *versus* the SN (30 μg total protein), short-exposure images confirmed that the increase in protein succination was only evident in the BS of Ndufs4 KO mice (see band at ~35 kDa), whereas no differences were observed in the SN (supplemental Fig. S1D, right panel). Notably, the lower protein loading used in this experiment suggested that although tubulin succination is present under normal conditions it does not increase in the KO BS. Overall, these data confirm that only select proteins in specific brain regions associated with pathology are succinated in the KO mouse. Increased protein succination occurs specifically as a result of fumarate reactivity with protein thiols (1, 2, 6–12). We examined fumarate levels in the brainstem of WT *versus* Ndufs4 KO mice at ~55 days, however fumarate levels were not increased (data not shown). This suggests that the increase in fumarate that contributes to succination may occur at an earlier time point prior to the accumulation of succinated proteins (and perhaps only in select regions), as we have observed previously in the 3T3-L1 adipocyte model (2). However, to demonstrate that increased fumarate leads to succination in neurons, we used a lentiviral vector containing
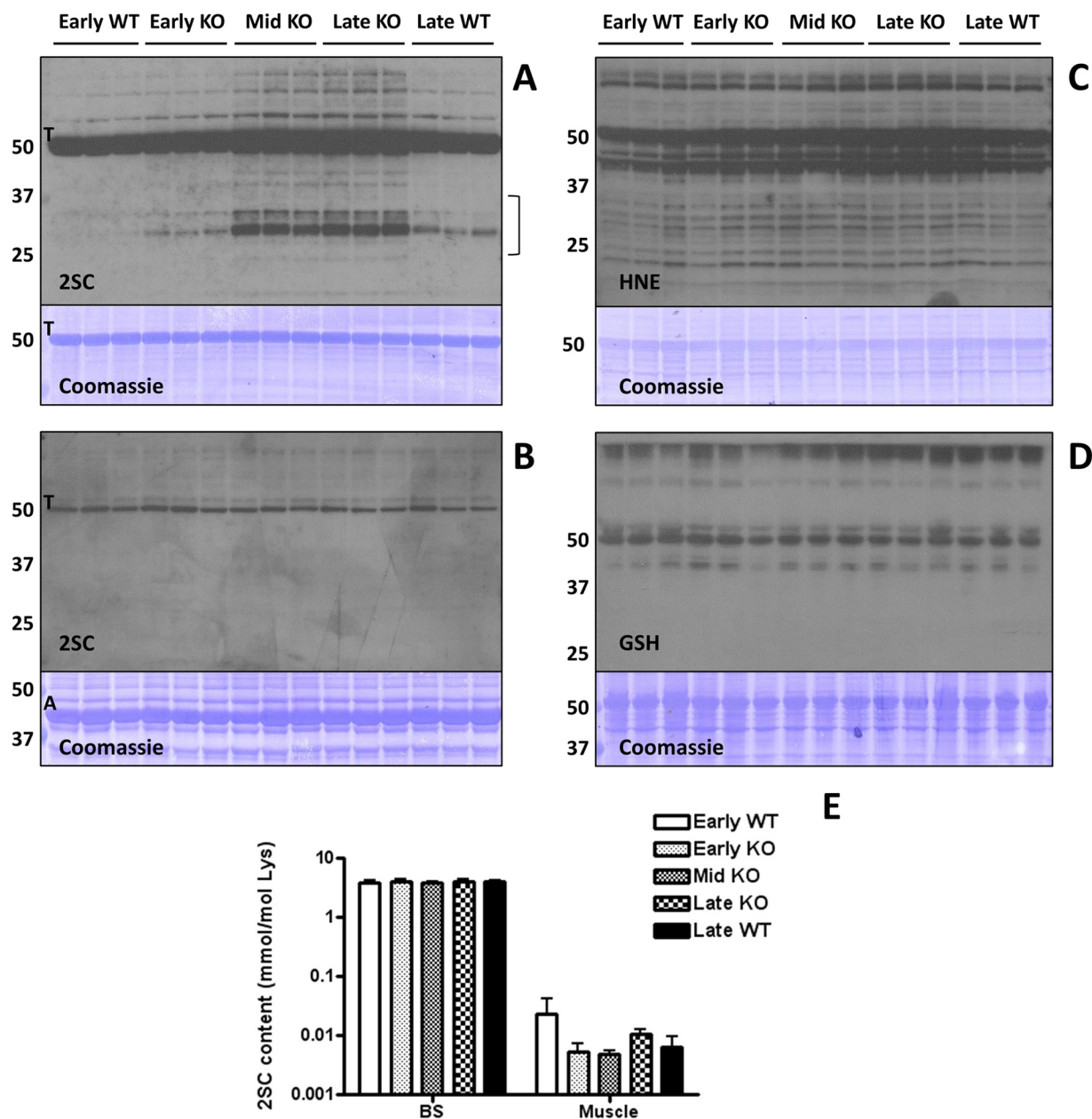
FIG. 1. **Protein succination is increased in the brainstem (BS) of Ndufs4 KO mice.** *A*, Total cell lysates (30 µg protein) from BS of early (3 weeks old), middle (Mid, 6 weeks old) and late (9 weeks old) WT and Ndufs4 KO mice were separated by SDS/PAGE, and succinated proteins were detected using a polyclonal anti-2SC antibody (2SC panel), as described under "Experimental Procedures." Protein succination in the BS of KO mice increased in association with the age of the mice and progression of disease *versus* WT controls. Succination was detected on a range of proteins and is especially prominent for proteins of ~70–80 and ~25–35 kDa (2SC panel). Note that intense tubulin (T) succination is present in all the lanes, and seems to increase with age in the BS of Ndufs4 KO mice. The bracket denotes the area circled in Fig. 3*B*. *B*, Succination of proteins is unchanged in skeletal muscle of Ndufs4 KO mice. Note that even when actin (*A*) is much more abundant (Coomassie panel), tubulin (T) is the primary succinated protein, confirming the selectivity of the modification. The identity of the tubulin band was confirmed in the BS by LC-MS/MS. *C*, Protein modification by the reactive lipid peroxidation product 4-hydroxy-2-nonenal (HNE) and (*D*) glutathione (GSH) is unchanged in the BS of Ndufs4 KO mice. *E*, The total 2SC content of BS and muscle was determined by GC-MS/MS after acid hydrolysis of the protein. Note that 2SC content (expressed as mmol/mol lysine) is much higher in BS than in muscle. Results are presented as mean ± S.E. No significant differences between ages and genotypes were observed. In all the panels, triplicate samples were used for each age and genotype. In *A*, *B*, *C*, and *D* molecular masses of marker proteins are indicated on the left-hand side.
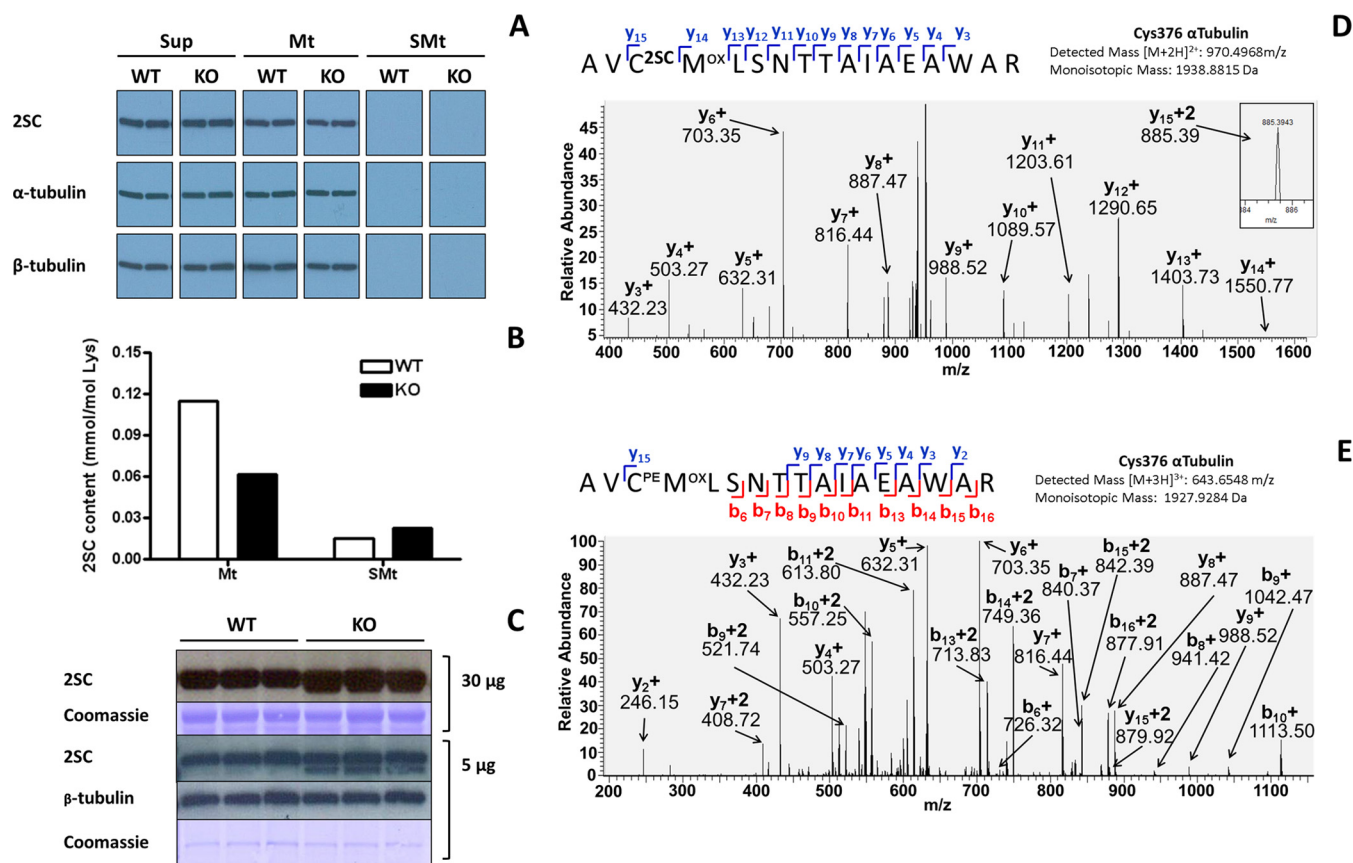
FIG. 2. **Endogenous succination does not alter tubulin polymerization in the brainstem of WT and Ndufs4 KO mice.** *A*, BS samples were homogenized and centrifuged to obtain a cleared supernatant (Sup) as described under "Experimental Procedures." When Sup was subjected to polymerization in the presence of taxol and high speed centrifugation, succinated tubulin (2SC panels) appeared in the microtubule pellet (Mt) but not in the remaining supernatant (SMt). Tubulin subunits (α-tubulin and β-tubulin panels) followed exactly the same pattern of distribution, indicating that endogenous succination of tubulin did not impair polymerization. Duplicate samples are shown for each genotype in this experiment; the same results were obtained in another experiment using a different set of samples. *B*, Total 2SC content (in mmol/mol Lys) was determined in Mt and SMt fractions after tubulin polymerization of BS samples by GC-MS/MS as described under "Experimental Procedures." The distribution of succinated proteins favors the Mt fractions, especially in the BS of WT mice, whereas the BS of KO mice show a trend to increased total succination in the SMt fractions. Results are shown as the average of duplicate samples. *C*, Protein succination in the ~50 kDa region of BS extracts from WT and Ndufs4 KO mice. For 30 μg protein samples succination increases in the KO group (30 μg, 2SC panel), but a slightly lower MW band is present in all samples (30 μg, Coomassie panel). With a reduced protein load of 5 μg, succination increases for the lower MW band in the BS of KO mice, with no changes in tubulin succination (5 μg, 2SC panel). β-tubulin and Coomassie staining are included to show even loading of the lanes (5 μg, β-tubulin and Coomassie panels). *D–E*, Cys$^{376}\alpha$ is a prominent site of succination in the BS of the mouse. Mt fractions were resolved by SDS/PAGE and the tubulin bands at ~50 kDa were excised and digested with trypsin prior to LC-MS/MS analysis as detailed under "Experimental Procedures." *D*, MS/MS sequencing showing succination of Cys$^{376}\alpha$ (C^{2SC}) in the peptide AVCMLSNTTAIAEAWAR; the pyridylethylated version of Cys$^{376}\alpha$ (C^{PE}) is shown in (*E*).

either fumarase (*Fh1*) or scrambled control shRNA to knock down fumarase levels (leading to specific fumarate accumulation) and increased protein succination in differentiated N1E-115 neurons (supplemental Fig. S1*E* and S1*F*). This confirms that accumulation of fumarate (~18-fold in this model) in neurons contributes to succination of reactive protein thiols.

We also determined the total 2SC content in muscle and brain areas of WT and Ndufs4 KO mice by GC-MS/MS after acid hydrolysis of the proteins. Fig. 1*E* demonstrates that the 2SC content was ~1000-fold higher in BS compared with muscle, confirming the anti-2SC immunoblot data for these tissues (Fig. 1*A* and 1*B*). However, no differences in 2SC content were observed because of age or genotype, which may be attributed to the elevated levels of basal tubulin succination masking the immunologically detected changes in lesser abundant succinated proteins in the KO. For the same reasons, 2SC content in other brain areas, while elevated *versus* muscle 2SC levels, remained unchanged between genotypes (supplemental Fig. S1*G*).

In a previous study we identified tubulin as a target of succination (12). We showed that *in vitro* incubation of purified porcine brain tubulin with either fumarate or the more reactive fumarate ester dimethylfumarate induced tubulin succination, resulting in decreased tubulin polymerization. However, we

also observed that basal levels of endogenous tubulin succination in the normal mouse brain did not interfere with tubulin polymerization. To extend these observations to the Ndufs4 KO model, we subjected BS extracts from WT and KO mice to tubulin polymerization in the presence of taxol, as described under "Experimental Procedures." Fig. 2*A* shows that succinated tubulin (2SC, upper panel), α-tubulin (middle panel) and β-tubulin (lower panel) were present in the cleared initial supernatant (Sup), presumably as unpolymerized tubulin. When Sup was subjected to polymerization in the presence of taxol, the majority of succinated, α- and β-tubulin was incorporated into the microtubular pellet (Mt), as no immunoreactive bands for either 2SC or tubulin isoforms were detected in the supernatant after polymerization (SMt). Notably, no differences were observed between genotypes. These results indicate that the endogenous levels of tubulin succination do not interfere with tubulin polymerization in the presence of taxol in both the WT and KO BS. We also measured the total content of 2SC in the purified Mt and SMt fractions by GC-MS/MS. Interestingly, the amount of 2SC detected in Mt appeared to be reduced in the BS of Ndufs4 KO mice compared with WT, although these changes were not detected in the immunoblot (Fig. 2*A*). In contrast, the 2SC content was increased in the SMt fraction of Ndufs4 KO mice, suggesting that increases in succination of other proteins can be detected when the sample has been depleted of tubulin (Fig. 2*B*).

As tubulin polymerization was unaffected in the BS of KO mice, we re-examined tubulin succination using the protein amount we have used previously for immunoblots (30 μg, Fig. 1*A*) *versus* a much lower protein amount (5 μg). Fig. 2*C* indicates that the succinated band at ~50–55 kDa (30 μg, 2SC panel) appears to be larger in the BS of Ndufs4 KO mice compared with WT littermates, confirming the results shown in Fig. 1*A*. However, when the protein load was just 5 μg, the succinated band at ~50–55 kDa (Fig. 2*C*, 5 μg, 2SC panel) was resolved into two thinner bands. The upper band was equally succinated in BS from WT and Ndufs4 KO, and co-localizes with β-tubulin (Fig. 2*C*, 5 μg, β-tubulin panel). Importantly, the lower band was succinated only in the BS of KO mice (Fig. 2*C*, 5 μg, 2SC panel). This confirms our findings in Fig. 2*A* demonstrating that tubulin succination is not increased in the BS of the Ndufs4 KO; instead a different protein is succinated and this is specific to the KO.

We have previously identified several cysteine sites of succination by mass spectrometry when purified porcine brain tubulin is incubated with fumarate, including Cys347α, Cys$^{376}\alpha$, Cys$^{12}\beta$ and Cys$^{303}\beta$. The relative abundance of succination at these cysteines increased in association with increasing fumarate concentration (12). In the current study we proceeded to identify the sites of endogenous succination of tubulin in the BS of Ndufs4 KO mice. Microtubules (Mt, 100 μg) obtained after tubulin polymerization in the presence of taxol were subjected to SDS-PAGE separation and in-gel digestion with trypsin as described under "Experimental Pro-

cedures." Supplemental Table S1 confirms that α-tubulin is present in the Mt preparation, as numerous α-tubulin peptides from *Mus musculus* were identified following data-dependent MS/MS (64% sequence coverage). However, the lesser abundant succinated peptides were not identified in the initial data-dependent analysis of the sample. Further CID-MS/MS analysis of select cysteine containing precursor masses was used to look for either the succinated or pyridylethylated forms of the peptides. Cys^{376} was identified as a site of α-tubulin succination endogenously occurring in the BS of Ndufs4 KO mice, confirmed after assignment of the y^{15} fragment ion indicating the mass addition of 116.01 (fumarate) to Cys$^{376}\alpha$ (Fig. 2*D* shows the spectrum in the KO BS). Unsuccinated Cys$^{376}\alpha$ was also detected as the pyridylethylated product (Fig. 2*E* shows the spectrum in KO BS). In addition, Cys$^{347}\alpha$ was also found in both succinated and pyridylethylated forms (supplemental Fig. S2*A* and S2*B*, respectively, for the KO BS).

2-dimensional (2D) SDS-PAGE separation following isoelectric focusing (pI 4–7) was employed to further resolve the succinated proteins in the BS of Ndufs4 KO mice. The anti-2SC antibody detected many succinated proteins that were either increased or uniquely detected in the KO BS (Fig. 3*B versus* 3*A*), and there was abundant succination on a series of protein spots resolved at ~ 25–35 kDa, with isoelectric points ranging from ~ 5.5 to 7.0 (region highlighted by the dotted oval line in Fig. 3*B*). This region corresponds to the area denoted by the bracket on the far right of the 2SC panel in Fig. 1*A* that showed increased succination in the BS of Ndufs4 KO *versus* WT mice.

Initially, we focused our attention on DJ-1/park7 as one of the possible targets of succination in the BS of Ndufs4 KO mice for several reasons. First, DJ-1 functions as a redox chaperone that contains a cysteine (Cys^{106}) that can be oxidized to the sulfinic acid to facilitate neuroprotection (43). Therefore loss of this protective thiol may render the cells more susceptible to oxidative insults. Second, mutations in DJ-1 and two other proteins, PINK1 and parkin, are responsible for the majority of cases of autosomal recessive, early-onset Parkinson disease, a neurodegenerative disorder that produces progressive loss of dopaminergic neurons in the substantia nigra (44). Finally, we identified Cys^{106} of DJ-1 as one of the succinated sites in adipocytes grown in high glucose/high insulin media (45). This site is also succinated in HLRCC caused by fumarate hydratase deficiency, in which case the intracellular fumarate concentration is increased (11, 46). Our 2D blots show some colocalization of DJ-1 and succinated spots in the BS of Ndufs4 KO mice (Fig. 3*B* and 3*D*, designated by solid ovals), but DJ-1 succination was limited compared with other more intense 2SC-positive spots, suggesting that is not the most abundant succinated target in this model. Interestingly, the more acidic DJ-1 spots appear to increase in the BS of Ndufs4 KO (Fig. 3*D versus* 3*C*),
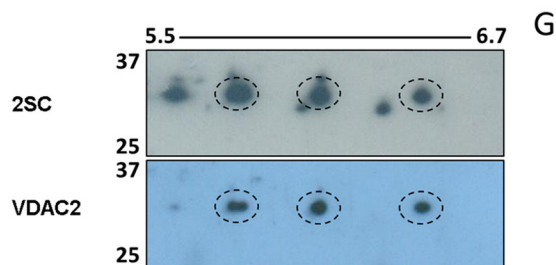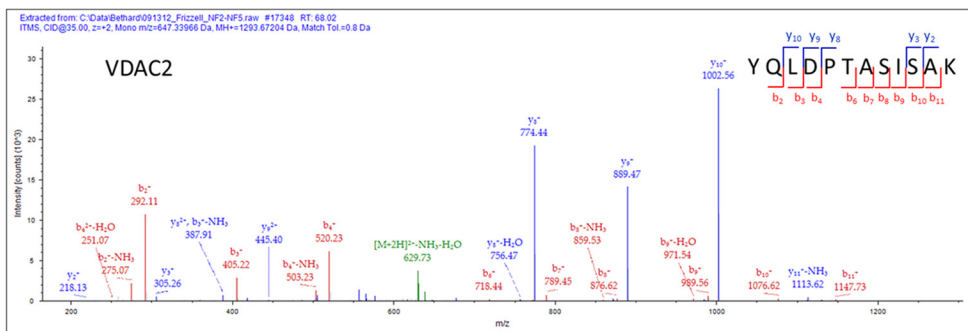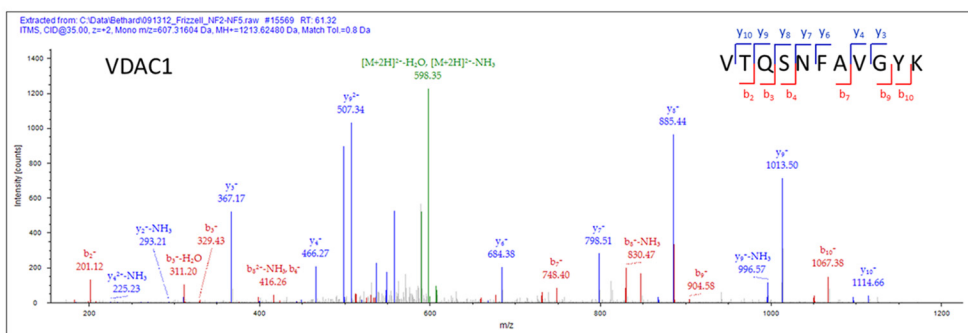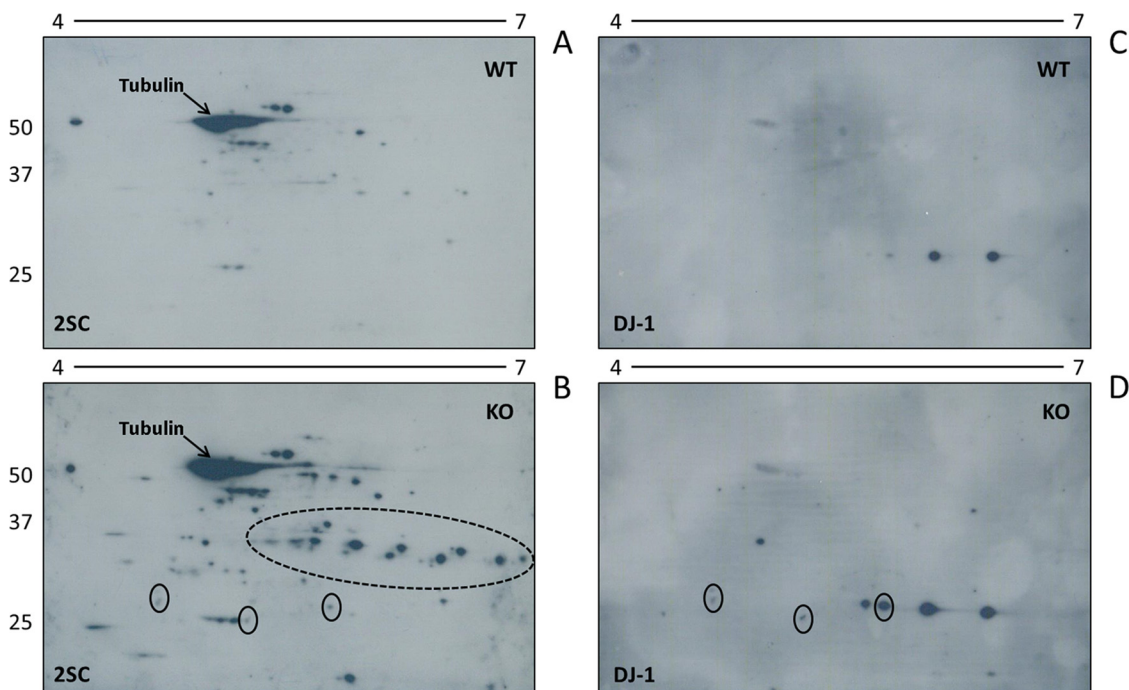
indicating a possible increase in the oxidation state of this redox chaperone.

To better characterize the nature of the more prominent succinated proteins in the BS of Ndufs4 KO mice, parallel 2D gels were prepared; one of these was transferred to a membrane and immunoblotted with the anti-2SC antibody and the other was stained with colloidal Coomassie blue for spot picking. Following the alignment of the gel and the blot, the succinated spots of interest were mapped and excised from the gel prior to trypsin digestion and identification by LC-MS/MS, as described under "Experimental Procedures." The most prominent proteins identified from the corresponding succinated spots located within the dotted oval in Fig. 3*B* were two isoforms of the voltage dependent anion channel (VDAC); VDAC1 and VDAC2. Supplemental Table S2 confirms the identification of peptides for both isoforms of VDAC (up to 55.7% sequence coverage), with many of the peptides being identified on multiple occasions. The sequenced spectrum for a manually validated representative peptide of each isoform (V^{177}TQSNFAVGYK^{187}, VDAC1 and Y^{237}QLDPTASISAK^{248}, VDAC2) is shown in Figs. 3*E* and 3*F*. We next validated the identification of the VDAC2 isoform as a succinated target protein using an anti-VDAC2 antibody. Fig. 3*G* illustrates the precise overlap of three VDAC2 immunoreactive spots (Fig. 3*G*, lower panel) with a specific subset of succinated spots in the ~5.7–6.5 pI range, as defined by the anti-2SC staining present in only the BS of Ndufs4 KO mice (Fig. 3*G*, upper panel). Prior to the above immunoblotting for VDAC2, this blot was probed with the anti-HNE antibody and no immunoreactivity was detected (data not shown), confirming the selectivity of succination for VDAC protein thiols.

The most pathologically affected regions of the brain in Ndufs4 KO mice include the vestibular nuclei (VN), the inferior olive/gigantocellular reticular nucleus (IO/Gi) of the BS, and the deep cerebellar fastigial nucleus (FN) (28, 47). To test if protein succination was specifically increased in these areas of the brain, we obtained micropunches of VN, IO/Gi, and FN from 400 μm brain slices; we also included micropunches from the typically unaffected crus 1 ansiform lobule (Crus 1) of the cerebellum as negative control. Although protein succination was increased in Ndufs4 KO mice in all the areas studied, succination was increased on many more proteins in the VN and IO/Gi (Fig. 4*A*, 2SC panel). More specifically, bands located at ~110, ~95, ~80, ~45, ~37, ~34, ~32, and ~30 kDa were all more heavily succinated in the VN and IO/Gi of Ndufs4 KO mice, whereas more discrete increments in succination were present in the FN (bands at ~110, ~45 and ~30 kDa). Marginal changes were observed in Crus 1, but these appeared to relate to total protein content (see VDAC1 and α-tubulin panels), rather than true increases in succination. This data highlights that increased succination is associated with the sites of greatest pathology, similar to our observations in Fig. 1. Shorter exposures confirmed that the succination status of the intense tubulin band (~50–55 kDa) was not affected by genotype in any of the regions studied (data not shown), validating the findings in Figs. 2*A* and 2*C*. The blots were subsequently probed with an anti-VDAC1 antibody, this confirmed co-localization of the VDAC1 protein with a ~32 kDa anti-2SC immunoreactive band, and additionally confirmed that the pronounced increases in succination in the VN and IO/Gi of the KO were not because of increased protein levels of VDAC1 (Fig. 4*A*, 2SC and VDAC1 panels). We have also confirmed that the total protein levels of VDAC2 do not change with the genotype (data not shown). Immunoblotting with an antibody to α-tubulin demonstrated equal loading of the lanes within each region (Fig. 4*A*, α-tubulin panel).

We then narrowed our focus based on the observations in the VN, considering that these nuclei are involved in respiratory control and knowing that the Ndufs4 KO mice commonly die because of respiratory failure (47). We again used isoelectric focusing (pI 4–7) followed by 2D SDS-PAGE separation to better examine the succinated proteins in the VN of Ndufs4 KO mice. Our 2D immunoblots show a considerable increase in protein succination in the VN of Ndufs4 KO mice *versus* the WT, again this is most pronounced in the ~25–35 kDa region (Fig. 4*B* and C, WT and KO 2SC panels). We observed a striking co-localization of protein succination with immunoreactivity to antibodies for both VDAC1 and VDAC2 in the VN of Ndufs4 KO mice (Fig. 4*B* and 4*C*, note dashed lines surrounding VDAC1and VDAC2 blots and corresponding regions in the 2SC panels). Note that both isoforms of VDAC overlap with three succinated spots in the KO VN, whereas the overlap in

FIG. 3. **VDAC1 and 2 are succinated in the brainstem of Ndufs4 KO mice.** Protein (200 μg) from late stage (~9 week old) WT and Ndufs4 KO BS was isoelectrically focused across a 4–7 pH range, followed by 2D electrophoresis and immunoblotting as described under "Experimental Procedures." *A–B*, Increased succination was observed for a large number of proteins in the KO (panel *B*) *versus* WT (panel *A*) BS. The series of 2SC spots in the ~25–35 kDa region (dashed oval in *B*) corresponds to the region in the bracket in Fig. 1*A*, where a significant increase in succination was observed in the KO BS. This series of spots was analyzed by mass spectrometry to identify succinated proteins (see *E* and *F*). The abundance of 2SC-tubulin is labeled (arrows). *C–D*, After stripping the blots shown in A and B, probing was performed with a DJ-1 antibody. Some overlapping with 2SC immunoreactivity was observed, suggesting DJ-1 succination (solid ovals). *E–G*, Duplicate 2D gels from WT and KO BS were stained with Coomassie blue, or transferred to PVDF for immunoblotting with our 2SC antibody (*G*, upper panel) and after stripping with an antibody to VDAC2 (*G*, lower panel). Spot picking from stained gels in the ~25–35 kDa region using the 2SC blot as a guide, followed by in-gel digestion and MS/MS analysis allowed for the identification of VDAC1 and VDAC2 as prominent succinated proteins (see supplemental Table S2 for identified sequences). The MS/MS spectra for two specific peptides are shown in *E*, VTQSNFAVGYK for murine VDAC1 (MH$^+$ = 1213.62480); and *F*, YQLDPTASISAK for murine VDAC2 (MH$^+$ = 1293.67204). There is precise overlap between several 2SC-modified spots and those identified by anti-VDAC2 (dashed ovals, *G*). In *A*, *B*, *C*, *D*, and *G*, molecular masses of marker proteins are indicated on the left-hand side.
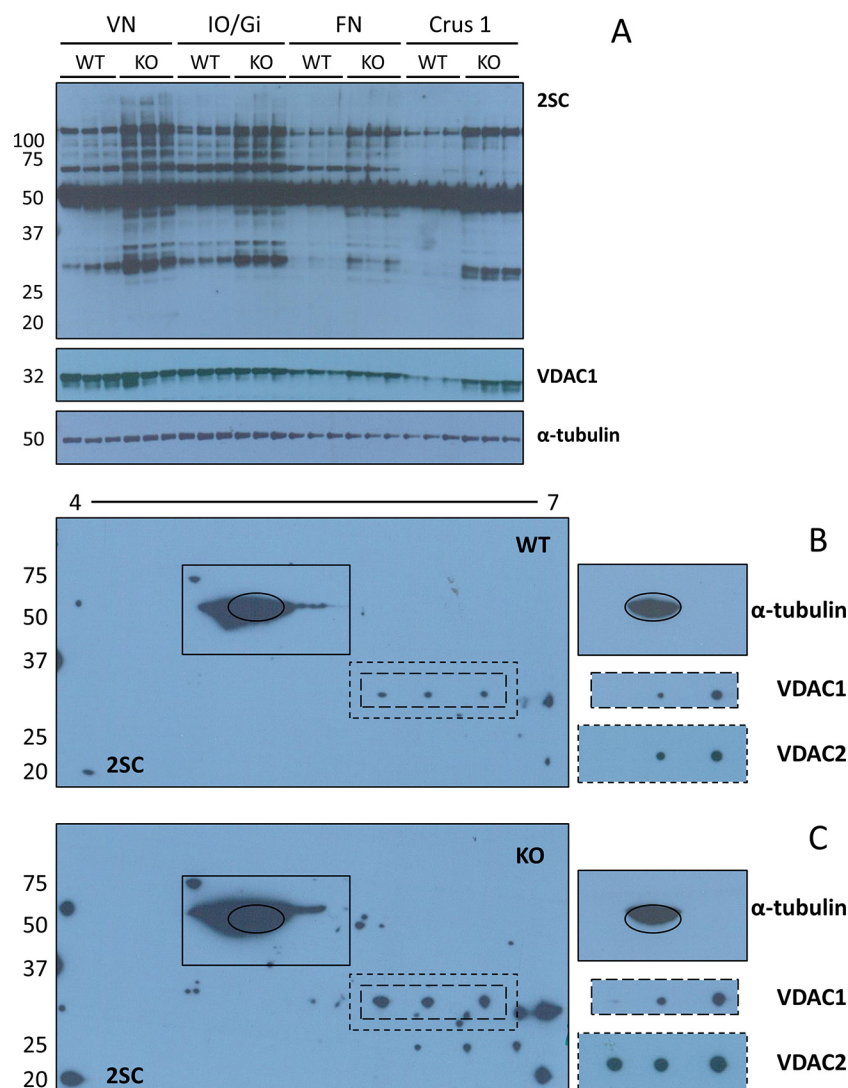
FIG. 4. **Protein succination is increased in brainstem and cerebellar nuclei of Ndufs4 KO mice.** *A*, Micropunches obtained from the vestibular nuclei (VN) and inferior olive/gigantocellular reticular nucleus (IO/Gi) of the BS, and the fastigial nucleus (FN) and crus 1 ansiform lobule (Crus 1) of the CB were homogenized, and proteins separated by SDS-PAGE. Probing with the anti-2SC antibody revealed increased protein succination in all the regions in the Ndufs4 KO mice, particularly in the BS nuclei (2SC panel). VDAC1 immunoreactivity (VDAC1 panel) shows overlap with a band at ~32 kDa that is more succinated in the BS nuclei of Ndufs4 KO mice. α-tubulin was used as a loading control (α-tubulin panel). *B, C*, Protein (150 μg) from late stage WT and Ndufs4 KO VN was isoelectrically focused across a 4–7 pH range, followed by 2D electrophoresis and immunoblotting as described under "Experimental Procedures." 2D blots show a considerable increase in protein succination in the VN of Ndufs4 KO mice (*C*, 2SC panel), particularly in the ~25–35 kDa region. Co-localization of VDAC1 immunoreactivity with protein succination occurs in both WT (*B*, VDAC1 and 2SC panels) and Ndufs4 KO (*C*, VDAC1 and 2SC panels), but the degree of succination is increased in VN of KO mice. The profile is similar for VDAC2, with a third spot of colocalization in Ndufs4 KO VN (*C*, VDAC2 and 2SC panels). α-tubulin (highlighted with a black oval) shows a similar pattern of succination (*B* and *C*, 2SC and α-tubulin panels). Molecular masses of marker proteins are indicated on the left-hand side.

the WT VN occurs for only two spots (Fig. 4*B* and 4*C*), suggesting that increased succination increases the acidity of the protein. Succination of α-tubulin appears to be unchanged in the VN of Ndufs4 KO *versus* WT mice (Fig. 4*B* and 4*C*, solid lines surrounding anti-tubulin blot and corresponding region in 2SC panel).

Finally, we used high resolution mass spectrometry to identify the endogenous sites of VDAC succination in the brainstem of the Ndufs4 KO. In order to first identify the sites

susceptible to fumarate modification we prepared a mitochondrial-enriched fraction from WT mouse brain cortex and subjected this to *in vitro* succination with fumarate to maximize the levels of succination. This was next separated by SDS-PAGE as described under "Experimental Procedures" and the bands at ~30–35 kDa were excised and digested with trypsin prior to LC-MS/MS. The presence of VDAC2 in the bands was initially confirmed, as several peptides from murine VDAC2 were identified (supplemental Table S1, se-
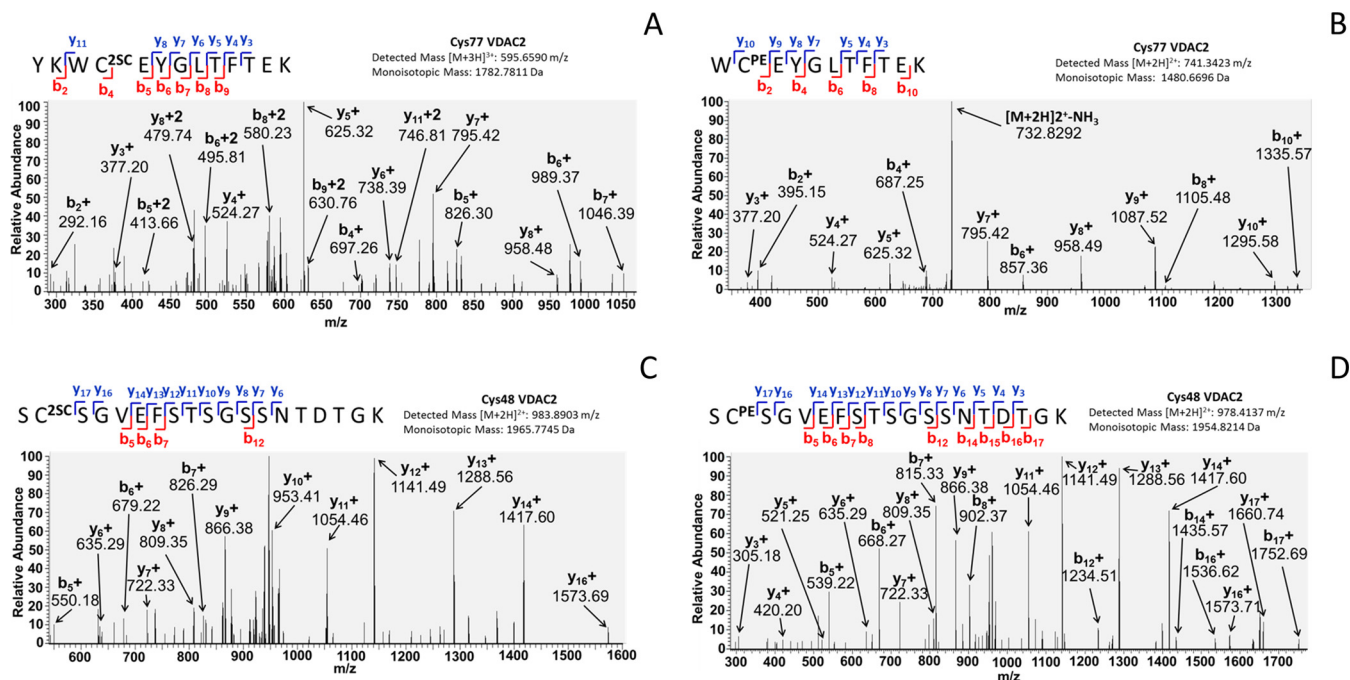
Fig. 5. **Identification of succination sites in VDAC2.** *A*, *B*, Mitochondrial-enriched fractions from Ndufs4 KO mouse brainstem were resolved by SDS-PAGE, gels were stained with Coomassie Brilliant Blue, bands at ~30–35 kDa were excised, destained and digested with trypsin as described under "Experimental Procedures." MS/MS spectra showing that Cys[77] in the peptide YKWC^{2SC}EYGLTFTEK of VDAC2 is endogenously succinated *in vivo* (*A*); the unmodified Cys[77] in the peptide WC^{PE}EYGLTFTEK was also identified after alkylation with 4-vinylpyridine (*B*). *C*, *D*, MS/MS spectra showing that Cys[48] in the peptide SC^{2SC}SGVEFSTSGSSNTDTGK of VDAC2 is endogenously succinated *in vivo* (*C*); the unmodified Cys[48] in the peptide SC^{PE}SGVEFSTSGSSNTDTGK was also identified after alkylation with 4-vinylpyridine (*D*).

quence coverage: 50.88%). We subjected several predicted cysteine containing precursor ion masses (succinated or pyridylethylated) to CID-MS/MS and identified the primary sites of *in vitro* VDAC2 succination as Cys[77] and Cys[104] (supplemental Fig. S3*A* and S3*C*, respectively). Unsuccinated Cys[77] and Cys[104] were also detected as pyridylethylated cysteines (supplemental Fig. S3*B* and S3*D*, respectively). Having demonstrated potential sites of VDAC succination *in vitro*, we then searched for sites of VDAC2 succination in mitochondrial-enriched fractions obtained from Ndufs4 KO BS. We detected the +3 charge-state peptide for succinated Cys[77] (595.6590 m/z) (Fig. 5*A*), confirming that VDAC2 succination occurs *in vivo* in the BS of Ndufs4 KO mice. We also detected the unsuccinated (pyridylethylated) form of the peptide containing Cys[77] in the Ndufs4 KO brainstem (Fig. 5*B*). In addition, we confirmed that VDAC succination endogenously occurs *in vivo* on Cys[48], as we detected the +2 charge-state peptide for succinated Cys[48] (983.8903 m/z) (Fig. 5*C*, as well as the unsuccinated (pyridylethylated) form of the Cys[48] peptide (Fig. 5*D*) in the BS of Ndufs4 KO mice. Collectively, our results confirm that several cysteine residues on VDAC isoforms, particularly VDAC2, are targets of succination in the BS of the Ndufs4 KO mouse.

DISCUSSION

Protein succination refers to the formation of an irreversible thioether linkage between a cysteine residue and the mito-

chondrial metabolite fumarate (1, 2, 45). Increased succination in biological samples is restricted to situations where fumarate concentrations are significantly increased, for example, 2SC levels are specifically increased in cancers derived from fumarate hydratase mutations (6, 8), and in the metabolically overwhelmed adipocyte in type 2 diabetes (4, 5, 9). Glucotoxicity driven mitochondrial stress in the adipocyte prevents the oxidation of NADH, facilitating the accumulation of fumarate because of the inhibition of the Krebs cycle NAD$^+$-dependent dehydrogenases (9). In the current study we hypothesized that certain OXPHOS deficiencies may also result in a reduced capacity to re-oxidize NADH, thereby leading to increases in fumarate concentrations and ultimately protein succination. Our hypothesis was further supported by the correlation between urinary fumarate measurements and the presence of certain OXPHOS deficiencies in a retrospective metabolomic study (29). We tested our hypothesis in the Ndufs4 KO mouse, an animal model of Leigh syndrome and one of the most prevalent OXPHOS deficiencies in humans. These mice show remarkable similarities to the human disease, with symptoms that include ataxia, seizures, dystonia, and respiratory failure (28). Histologically, the brain of the Ndufs4 mouse shows changes that include decreased neuronal numbers, astrocyte and microglial proliferation (28, 47), and the accumulation of lipid droplets in both astrocytes and microglia (48). Strikingly, we observed clear increases in

brainstem protein succination that are apparent at 3 weeks of age (a period that precedes the disease symptoms) and increase progressively until the Ndufs4 KO mice die of respiratory failure at about 9 weeks (Fig. 1A). This is the first description of increased protein succination occurring in a neurological condition, specifically in mitochondrial disease. As protein succination appears to decrease the functionality of the target protein(s) (4, 8, 10–12), we predict that increased succination in the brain of the Ndufs4 KO mice will further decrease the already compromised mitochondrial function, suggesting that fumarate is a novel biochemical contributor to the progression of neuropathology.

In contrast to the brain, protein succination was not increased and was selectively present only on tubulin, despite the abundance of actin, in the skeletal muscle of the Ndufs4 KO *versus* WT mice (Fig. 1B). In support of this finding, we have shown that protein succination is not altered when myotubes are metabolically challenged by high glucose (12). In addition, succination levels in skeletal muscle do not change in the *db/db* model of type 2 diabetes, whereas adipose tissue succination is increased in the same model (5). Importantly, our results are in clear agreement with previous data showing that there is no major muscle pathology in Ndufs4 KO mice (27), and normal levels of pyruvate maximal oxidation and ATP production occur in skeletal muscle mitochondria isolated from these mice (49).

Our initial findings demonstrated that the brainstem (BS) shows increased protein succination in the Ndufs4 KO mouse (Fig. 1A). The BS is one of the sites where neurodegeneration is clearly prominent in these mice, and within this region, the vestibular nuclei (VN) are most affected (28, 47). When we used micropunches of BS tissue we confirmed that the VN is a major site of increased protein succination in the Ndufs4 KO mouse (Fig. 4). The VN complex serves as an integration center of sensory and motor information that regulates posture (50) and respiratory and cardiovascular responses to postural changes (51). Interestingly, both posture and respiration patterns are altered in the Ndufs4 KO mouse (47). We also studied the fastigial nucleus of the cerebellum, another region that shows histopathological changes in the Ndufs4 KO mouse (28, 47) and is involved in posture regulation (50). In this case, protein succination was moderately increased in the KO mice (Fig. 4A). Our results suggest that increased protein succination and loss of functionality in the VN and FN may play a direct role in the breathing irregularities and apneic episodes that lead to the respiratory failure linked deaths common to Leigh Syndrome. In addition, we also observed notable increases in protein succination in the inferior olive (IO)/gigantocellular reticular (Gi) region of the BS in Ndufs4 KO mice (Fig. 4A), another area that shows astrogliosis and microglial activation in this model (28). The IO provides inputs to the Purkinje cells in the cerebellar cortex (52); increased protein succination in this area could additionally contribute to the impaired movement control observed in the Ndufs4 KO

mouse. The Gi region is part of the bulbar gain setting system that receive sensory input and modulate motor output, and is affected in the initial states of Parkinson disease (53). Interestingly, Gi neurons also project to the VN (54, 55), suggesting that succination could affect the VN function via direct and indirect effects. In contrast the striatum (Str), a brain region that is not particularly affected in the Ndufs4 KO mouse in terms of morphology and neurochemistry (56), only showed moderate increases in protein succination in this model (supplemental Fig. S1C). In summary, these results clearly demonstrate the localization of increased protein succination with specific regions of the nervous system where histopathological anomalies have been described in the Ndufs4 KO mouse, whereas the skeletal muscle and brain areas that are devoid of pathology do not show changes in protein succination. Interestingly, studies in fibroblasts from the Ndufs4 KO mouse, which are not affected by pathology despite the loss of Ndufs4, only showed minor deficits in mitochondrial respiration with unchanged proliferation or cell survival (57, 58), further supporting the tissue specificity of our findings.

Increased levels of oxidative stress have been extensively described in mitochondrial diseases (28, 48, 59–62); however this is often ubiquitous and is not specific to the site of pathology (58, 59, 62). Moreover, the basal levels of reactive oxygen species are not increased in the dopaminergic neurons that innervate the striatum in the Ndufs4 KO mouse (56). In contrast to our data demonstrating that succination is specifically increased at the site of neuropathology in the Ndufs4 KO brain, we did not observe increased markers of oxidative stress in the BS of Ndufs4 KO mice, represented by the unchanged levels of both HNE conjugation to proteins (Fig. 1C) or glutathionylation of proteins (Fig. 1D). However, there appears to be a role for lipid peroxidation in the pathology of this model of Leigh syndrome, as lipid droplet accumulation in astrocytes and microglia in the BS and olfactory bulb (OB) precedes neurodegeneration and antioxidant therapy seems to delay symptoms onset, though this positive effect is transient (48). This suggests that oxidative stress is one component of the mitochondrial dysfunction; however, it is probably not the only contributor to the development of pathology in mitochondrial disease. Moreover, this explains why antioxidant therapies alone are insufficient to treat MD; rather, strategies that improve mitochondrial function will be necessary to counter the OXPHOS deficiency.

We have previously identified tubulin as a major target of succination in adipocytes grown in high glucose/high insulin concentrations, as well as in adipose tissue from diabetic mice (12). Furthermore, increased *in vitro* succination of tubulin with fumarate or dimethylfumarate decreases its polymerization (12). Initially, we suspected that tubulin succination was increased (Fig. 1A), but further investigation using lower protein loading demonstrated the presence of a lower molecular weight band that was succinated only in KO mice. The endogenous levels of succinated tubulin appeared un-

changed by immunoblotting in the BS of WT *versus* Ndufs4 KO mice (Figs. 2C and 3B). In agreement with these results, we did not detect changes in tubulin polymerization in the presence of taxol (Fig. 2A); taxol is required when tubulin polymerization from frozen tissue is studied (34). Interestingly, tubulin polymerization is not affected in nigrostriatal neurons of Ndufs4 KO mice under basal conditions, but rotenone addition increases dopamine accumulation and oxidation, and reduces tubulin polymerization, indicating that tubulin or microtubule interacting protein(s) functionality could be affected in this model in the presence of additional mitochondrial stress (63). We have detected the succinated residues $Cys^{347}\alpha$ and $Cys^{376}\alpha$ in the Ndufs4 KO BS (Fig. 2D and 2E and supplemental Figs. S2A and S2B). We have previously identified these residues as the primary succinated cysteines in α-tubulin after *in vitro* incubation of purified porcine brain tubulin with fumarate (12). These residues have also been documented to react rapidly with other thiol modifying agents, such as iodoacetamide and N-ethylmaleimide (64). $Cys^{347}\alpha$ is the most reactive exposed cysteine in the tubulin dimer (64), and is also the primary target for tubulin modification by isothiocyanates (65); whereas $Cys^{376}\alpha$ is less exposed but is documented to be modified by palmitoylation (66, 67). Overall, the presence of basal succination in WT as well as Ndufs4 KO BS may interfere with tubulin interactions with other proteins (namely microtubule associated proteins and molecular motors), or alter the subcellular localization of tubulin by competing with palmitoylation.

We used 2D-gel electrophoresis to better resolve the succinated proteins and this allowed us to specifically select the most succinated fraction of the total BS to confirm the protein identification, as the enrichment of post-translational modifications can be limited by the amount of protein modified. Ongoing studies in our laboratory are directed at optimizing chemical enrichment strategies that will permit the identification of other lesser abundant succinated proteins. We confirmed increased protein succination in the BS of Ndufs4 KO mice in the same molecular weight range as that observed in 1D gels (Figs. 3B and 1A, respectively). Initially, we were interested in the protein DJ-1 as a possible target for succination, as we previously described increased succination on the low pK_a (~5.4) Cys^{106} of this redox chaperone in adipocytes grown in high glucose/high insulin concentrations (45), and it is succinated in fumarate hydratase deficient kidney tumors (46). A meta-analysis of two-dimensional electrophoresis for DJ-1 has described the protein at two possible molecular weights, 20 and 25 kDa; and at pIs ranging from 6.3 to 7.2 (68). We detected DJ-1 at ~25 kDa (Fig. 3D), and some of the spots overlapped with our detection of succinated proteins in the same blot (Fig. 3B). Interestingly, the relative enrichment of more acidic isoforms of DJ-1 in the BS of Ndufs4 KO mice, irrespective of the succination state of the protein (Fig. 3D), is in clear agreement with similar findings in the brain of Parkinson disease patients (68), suggesting a

multiplicity of DJ-1 isoforms among different neurodegenerative diseases that warrants further investigation.

Spot-picking from duplicate 2D gels matched to the anti-2SC immunoblot was used to identify succinated protein targets, with an emphasis on the spots in the heavily succinated region ~30 kDa. With this approach, we successfully identified and confirmed the voltage dependent anion channel isoforms 1 and 2 (VDAC1 and 2, Figs. 3E–3G) in the Ndufs4 KO BS. Following this we isolated the VN and also confirmed by 2D blots with specific antibodies that VDAC1 and 2 were more succinated in the Ndufs4 KO mice compared with the same nuclei in WT mice (Fig. 4A–4C). VDACs are channels that span the mitochondrial outer membrane (69) and are the principal regulators of the flow of metabolites and ions, including ATP and ADP, earning them the title of 'mitochondrial governator' (70). Metabolite flow into and out of the mitochondria occurs when VDAC channels are open in the 'high-conductance' state (~0 mV potential) that is anion selective. This open state permits the movement of up to 2×10^6 ATP molecules/second and is favored as a result of the net positive charge in the channel lumen (71–73). The fact that we have confirmed pronounced increases in VDAC succination in a mitochondrial disease is particularly significant given the fact that these cells are already metabolically challenged. If succination alters VDAC channel activity this may further exacerbate the mitochondrial bioenergetic deficit. VDAC2 gene knockout is lethal (74), whereas knockout of isoforms 1 and 3 are not, suggesting important functional differences for the isoforms. VDAC2 is an abundant brain isoform (75) and is the most cysteine-rich isoform (11 cysteines in mouse, 9 cysteines in human), with most of them predicted to be located on exposed loops on the intermembrane space side of the channel and all of them in the reduced state and available for modification (76). In order to identify specific succinated target cysteines we first prepared *in vitro* succinated VDAC from mitochondrial tissue fractions from the brain, using these we confirmed Cys^{77} and Cys^{104} as target sites of succination for VDAC 2 (supplemental Fig. S3A and S3C, respectively). We then identified both Cys^{77} and Cys^{48} of VDAC2 as endogenously succinated sites in the BS of Ndufs4 KO mice (Fig. 5A and C). The confirmation of Cys^{77} succination in the brain supports the previous identification of succinated Cys^{77} in fibroblasts and kidneys from fumarate hydratase deficient mice in which intracellular fumarate concentrations are significantly increased (8). Although all VDAC isoforms do contain thiols that are exposed on the channel lumen, it was proposed that cysteine thiols do not appear to have a direct role in regulating channel conductance (77). However, nitrosylation of Cys^{127} on VDAC1 is predicted not only to decrease its conductance, but also to lock VDAC1 in a closed state (78). It is therefore possible that succination electrostatically alters the channel because of the introduction of negative charges. Indeed, the impact of charge modification on VDAC channel function has been shown previously as VDAC treatment with succinic anhydride,

which increases the negative charge of the channel, eliminates VDAC voltage-dependence and changes its selectivity from anion to cation (79). Further, VDAC phosphorylation leading to increased negative charge was shown to decrease the conductance of the channel, though the modified residue(s) were not identified (80, 81). It is also possible that the association of VDAC with modulatory proteins is altered when VDAC is succinated; an increase in the negative charge of the protein could *e.g.* disrupt the interaction of VDAC with tubulin (82), or VDAC2 interaction with Bak (83). Interestingly, Cys^{77}, Cys^{48} and Cys^{104} are all located on one side of the channel facing the intermembrane space and are all in close proximity, suggesting that charge differences on this side of the channel may alter intra-mitochondrial signaling, particularly that involving Bak/Bax (74, 83). In addition, Maurya *et al.* prepared a VDAC2 mutant replacing Cys^{47} with a glutamic acid (introducing 1 negative charge in that position). Interestingly this unique change in VDAC2 is predicted to decrease the pI from 7.44 to 6.81. This may have important implications for altering the protein:protein interactions in a given region, in addition to the predicted VDAC cysteine:lipid membrane interactions (76).

Overall, our novel biochemical and proteomic data confirm that protein succination is increased in brain regions where established pathological changes occur in the Ndufs4 KO mouse. The documentation that several cysteines in VDAC2 are succinated, and consequently negatively charged, suggests that anion selectivity may be impaired, ultimately leading to impaired mitochondrial ATP efflux in a cell that is already bioenergetically deficient, further contributing to reduced cytosolic ATP levels by decreasing mitochondrial ATP export.

Ⓢ This article contains supplemental Figs. S1 to S3 and Tables S1, S2.

‡‡ To whom correspondence should be addressed: Department of Pharmacology, Physiology & Neuroscience, School of Medicine, University of South Carolina, 6439 Garners Ferry Road, Columbia, SC 29209. Tel.: (803) 216-3521; Fax: (803) 216-3538; E-mail: norma.frizzell@uscmed.sc.edu.

REFERENCES

1. Alderson, N. L., Wang, Y., Blatnik, M., Frizzell, N., Walla, M. D., Lyons, T. J., Alt, N., Carson, J. A., Nagai, R., Thorpe, S. R., and Baynes, J. W. (2006) S-(2-Succinyl)cysteine: a novel chemical modification of tissue proteins by a Krebs cycle intermediate. *Arch. Biochem. Biophys.* **450,** 1–8

2. Nagai, R., Brock, J. W., Blatnik, M., Baatz, J. E., Bethard, J., Walla, M. D., Thorpe, S. R., Baynes, J. W., and Frizzell, N. (2007) Succination of protein thiols during adipocyte maturation: a biomarker of mitochondrial stress. *J. Biol. Chem.* **282,** 34219–34228

3. Lai, R. K., and Goldman, P. (1992) Organic acid profiling in adipocyte differentiation of 3T3-F442A cells: increased production of Krebs cycle acid metabolites. *Metabolism* **41,** 545–547

4. Frizzell, N., Rajesh, M., Jepson, M. J., Nagai, R., Carson, J. A., Thorpe, S. R., and Baynes, J. W. (2009) Succination of thiol groups in adipose tissue proteins in diabetes: succination inhibits polymerization and secretion of adiponectin. *J. Biol. Chem.* **284,** 25772–25781

5. Thomas, S. A., Storey, K. B., Baynes, J. W., and Frizzell, N. (2012) Tissue distribution of S-(2-succino)cysteine (2SC), a biomarker of mitochondrial stress in obesity and diabetes. *Obesity* **20,** 263–269

6. Bardella, C., El-Bahrawy, M., Frizzell, N., Adam, J., Ternette, N., Hatipoglu, E., Howarth, K., O'Flaherty. L., Roberts, I., Turner, G., Taylor, J., Giaslakiotis, K., Macaulay, V. M., Harris, A. L., Chandra, A., Lehtonen, H. J., Launonen, V., Aaltonen, L. A., Pugh, C. W., Mihai, R., Trudgian, D., Kessler, B., Baynes, J. W., Ratcliffe, P. J., Tomlinson, I. P., and Pollard, P. J. (2011) Aberrant succination of proteins in fumarate hydratase-deficient mice and HLRCC patients is a robust biomarker of mutation status. *J. Pathol.* **225,** 4–11

7. Chen, Y. B., Brannon, A. R., Toubaji, A., Dudas, M. E., Won, H. H., Al-Ahmadie, H.A., Fine, S. W., Gopalan, A., Frizzell, N., Voss, M. H., Russo, P., Berger, M. F., Tickoo, S. K., and Reuter, V. E. (2014) Hereditary leiomyomatosis and renal cell carcinoma syndrome-associated renal cancer: recognition of the syndrome by pathologic features and the utility of detecting aberrant succination by immunohistochemistry. *Am. J. Surg. Pathol.* **38,** 627–637

8. Ternette, N., Yang, M., Laroyia, M., Kitagawa, M., O'Flaherty, L., Wolhuter. K., Igarashi, K., Saito, K., Kato, K., Fischer, R., Berquand, A., Kessler, B. M., Lappin, T., Frizzell, N., Soga, T., Adam, J., and Pollard, P. J. (2013) Inhibition of mitochondrial aconitase by succination in fumarate hydratase deficiency. *Cell Rep.* **3,** 689–700

9. Frizzell, N., Thomas, S. A., Carson, J. A., and Baynes, J. W. (2012) Mitochondrial stress causes increased succination of proteins in adipocytes in response to glucotoxicity. *Biochem. J.* **445,** 247–254

10. Blatnik, M., Frizzell, N., Thorpe, S. R., and Baynes, J. W. (2008) Inactivation of glyceraldehyde-3-phosphate dehydrogenase by fumarate in diabetes: formation of S-(2-succinyl)cysteine, a novel chemical modification of protein and possible biomarker of mitochondrial stress. *Diabetes* **57,** 41–49

11. Adam, J., Hatipoglu, E., O'Flaherty, L., Ternette, N., Sahgal, N., Lockstone, H., Baban, D., Nye, E., Stamp, G. W., Wolhuter, K., Stevens, M., Fischer, R., Carmeliet, P., Maxwell, P. H., Pugh, C. W., Frizzell, N., Soga, T., Kessler, B. M., El-Bahrawy, M., Ratcliffe, P. J., and Pollard. P. J. (2011) Renal cyst formation in Fh1-deficient mice is independent of the Hif/Phd pathway: roles for fumarate in KEAP1 succination and Nrf2 signaling. *Cancer Cell* 20, 524–537

12. Piroli, G. G., Manuel, A. M., Walla, M. D., Jepson, M. J., Brock, J. W., Rajesh, M. P., Tanis, R. M., Cotham, W. E., and Frizzell, N. (2014) Identification of protein succination as a novel modification of tubulin. *Biochem. J.* 462, 231–245

13. Tucker, E. J., Compton, A. G., and Thorburn, D. R. (2010) Recent advances in the genetics of mitochondrial encephalopathies. *Curr. Neurol. Neurosci. Rep.* **10,** 277–285

14. Skladal, D., Halliday, J., and Thorburn, D. R. (2003) Minimum birth prevalence of mitochondrial respiratory chain disorders in children. *Brain* **126,** 1905–1912

15. Finsterer, J. (2008) Leigh and Leigh-like syndrome in children and adults. *Pediatr. Neurol.* **39,** 223–235

16. Rahman, S., Blok, R. B., Dahl, H. H., Danks, D. M., Kirby, D. M., Chow, C. W., Christodoulou, J., and Thorburn, D. R. (1996) Leigh syndrome: clinical features and biochemical and DNA abnormalities. *Ann. Neurol.* **39,** 343–351

17. Ruhoy, I. S., and Saneto, R. P. (2014) The genetics of Leigh syndrome and its implications for clinical practice and risk management. *Appl. Clin. Genet.* **7,** 221–234

18. Pagniez-Mammeri, H., Loublier, S., Legrand, A., Bénit, P., Rustin, P., and Slama, A. (2012) Mitochondrial complex I deficiency of nuclear origin I. Structural genes. *Mol. Genet. Metab.* **105,** 163–172

19. Pagniez-Mammeri, H., Rak, M., Legrand, A., Bénit, P., Rustin, P., and Slama, A. (2012) Mitochondrial complex I deficiency of nuclear origin II. Non-structural genes. *Mol. Genet. Metab.* **105,** 173–179

20. Mimaki, M., Wang, X., McKenzie, M., Thorburn, D. R., and Ryan, M. T. (2012) Understanding mitochondrial complex I assembly in health and disease. *Biochim. Biophys. Acta* **1817,** 851–862

21. van den Heuvel, L., Ruitenbeek, W., Smeets, R., Gelman-Kohan, Z., Elpeleg, O., Loeffen, J., Trijbels, F., Mariman, E., de Bruijn, D., and Smeitink, J. (1998) Demonstration of a new pathogenic mutation in human complex I deficiency: A 5-bp duplication in the nuclear gene encoding the 18-kD (AQDQ) subunit. *Am. J. Hum. Genet.* **62,** 262–268

22. Loeffen, J. L., Smeitink, J. A., Trijbels, J. M., Janssen, A. J., Triepels, R. H., Sengers, R. C., and van den Heuvel, L. P. (2000) Isolated complex I deficiency in children: clinical, biochemical and genetic aspects. *Hum. Mutat.* **15,** 123–134

23. Budde, S. M., van den Heuvel, L. P., Janssen, A. J., Smeets, R. J., Buskens, C. A., DeMeirleir, L., Van Coster, R., Baethmann, M., Voit, T., Trijbels, J. M., and Smeitink, J. A. (2000) Combined enzymatic complex I and III deficiency associated with mutations in the nuclear encoded NDUFS4 gene. *Biochem. Biophys. Res. Commun.* **275,** 63–68

24. Calvaruso, M. A., Willems, P., van den Brand, M., Valsecchi, F., Kruse, S., Palmiter, R., Smeitink, J., and Nijtmans, L. (2012) Mitochondrial complex III stabilizes complex I in the absence of NDUFS4 to provide partial activity. *Hum. Mol. Genet.* **21,** 115–120

25. Lazarou, M., McKenzie, M., Ohtake, A., Thorburn, D. R., and Ryan, M. T. (2007) Analysis of the assembly profiles for mitochondrial- and nuclear-DNA-encoded subunits into complex I. *Mol. Cell. Biol.* **27,** 4228–4237

26. Leshinsky-Silver, E., Lebre, A.S., Minai, L., Saada, A., Steffann, J., Cohen, S., Rötig, A., Munnich, A., Lev, D., and Lerman-Sagie, T. (2009) NDUFS4 mutations cause Leigh syndrome with predominant brainstem involvement. *Mol. Genet. Metab.* **97,** 185–189

27. Kruse, S. E., Watt, W. C., Marcinek, D. J., Kapur, R. P., Schenkman, K. A., and Palmiter, R. D. (2008) Mice with mitochondrial complex I deficiency develop a fatal encephalomyopathy. *Cell Metab.* **7,** 312–320

28. Quintana, A., Kruse, S. E., Kapur, R. P., Sanz, E., and Palmiter, R. D. (2010) Complex I deficiency due to loss of Ndufs4 in the brain results in progressive encephalopathy resembling Leigh syndrome. *Proc. Natl. Acad. Sci. U.S.A.* **107,** 10996–11001

29. Barshop, B. A. (2004) Metabolomic approaches to mitochondrial disease: correlation of urine organic acids. *Mitochondrion* **4,** 521–527

30. Franklin, K. B. J., and Paxinos, G. (2008) *The mouse brain in stereotaxic coordinates*, 3rd Ed., Academic Press, Elsevier, New York, NY

31. Frezza, C., Cipolat, S., Scorrano, L. (2007) Organelle isolation: functional mitochondria from mouse liver, muscle and cultured fibroblasts. *Nat. Protoc.* **2,** 287–295

32. Lowry, O. H., Rosenbrough, N. J., Farr, A. L., and Randall, R. J. (1951) Protein measurement with the Folin phenol reagent. *J. Biol. Chem.* **193,** 265–275

33. Kinter, M., Sherman, N. E. (2000) *Protein sequencing and identification using tandem mass spectrometry*, pp.147–165, Wiley Interscience, Inc., New York, NY

34. Miller, L. M., Xiao, H., Burd, B., Horwitz, S. B., Angeletti, R. H., and Verdier-Pinard, P. (2010) Methods in tubulin proteomics. *Methods Cell Biol.* **95,** 105–126

35. Butterfield, D. A., Bader Lange, M. L., and Sultana, R. (2010) Involvements of the lipid peroxidation product, HNE, in the pathogenesis and progression of Alzheimer's disease. *Biochim. Biophys. Acta* **1801,** 924–929

36. Perluigi, M., Coccia, R., and Butterfield, D. A. (2012) 4-Hydroxy-2-nonenal, a reactive product of lipid peroxidation, and neurodegenerative diseases: a toxic combination illuminated by redox proteomics studies. *Antioxid. Redox Signal.* **17,** 1590–1609

37. Sanders, L. H., and Greenamyre, J. T. (2013) Oxidative damage to macromolecules in human Parkinson disease and the rotenone model. *Free Radic. Biol. Med.* **62,** 111–120

38. Korotchkina, L. G., Yang, H., Tirosh, O., Packer, L., and Patel, M. S. (2001) Protection by thiols of the mitochondrial complexes from 4-hydroxy-2-nonenal. *Free Radic. Biol. Med.* **30,** 992–999

39. Pastore, A., Petrillo, S., Tozzi, G., Carrozzo, R., Martinelli, D., Dionisi-Vici, C., Di Giovamberardino, G., Ceravolo, F., Klein, M. B., Miller, G., Enns, G. M., Bertini. E., and Piemonte. F. (2013) Glutathione: a redox signature in monitoring EPI-743 therapy in children with mitochondrial encephalo-myopathies. *Mol. Genet. Metab.* 109, 208–214

40. Enns, G. M., Moore, T., Le, A., Atkuri, K., Shah, M. K., Cusmano-Ozog, K., Niemi, A. K., and Cowan, T. M. (2014) Degree of glutathione deficiency and redox imbalance depend on subtype of mitochondrial disease and clinical status. *PLoS ONE* **9,** 1–9

41. Hargreaves, I. P., Sheena, Y., Land, J. M., and Heales, S. J. (2005) Glutathione deficiency in patients with mitochondrial disease: implications for pathogenesis and treatment. *J. Inherit. Metab. Dis.* **28,** 81–88

42. Popov, D. (2014) Protein S-glutathionylation: From current basics to targeted modifications. *Arch. Physiol. Biochem.* **120,** 123–130

43. Canet-Avilés, R. M., Wilson, M. A., Miller, D. W., Ahmad, R., McLendon, C., Bandyopadhyay, S., Baptista, M. J., Ringe, D., Petsko, G. A., and Cookson, M. R. (2004) The Parkinson's disease protein DJ-1 is neuroprotective due to cysteine-sulfinic acid-driven mitochondrial localization. *Proc. Natl. Acad. Sci. U.S.A.* **101,** 9103–9108

44. van der Merwe, C., Dashti, Z. J. S., Christoffels, A., Loos, B., and Bardien, S. (2015) Evidence for a common biological pathway linking three Parkinson's disease-causing genes: *parkin*, *PINK1* and *DJ-1. Eur. J. Neurosci.* doi: 10.1111/ejn.12872. [Epub ahead of print]

45. Merkley, E. D., Metz, T. O., Smith, R. D., Baynes, J. W., and Frizzell, N. (2014) The succinated proteome. *Mass Spectrom. Rev.* **33,** 98–109

46. Yang, M., Ternette, N., Su, H., Dabiri, R., Kessler, B. M., Adam, J., Teh, B. T., and Pollard, P. J. (2014) The succinated proteome of FH-mutant tumours. *Metabolites* **4,** 640–654

47. Quintana, A., Zanella, S., Koch, H., Kruse, S. E., Lee, D., Ramirez, J. M., and Palmiter, R. D. (2012) Fatal breathing dysfunction in a mouse model of Leigh syndrome. *J. Clin. Invest.* **122,** 2359–2368

48. Liu, L., Zhang, K., Sandoval, H., Yamamoto, S., Jaiswal, M., Sanz, E., Li, Z., Hui, J., Graham, B. H., Quintana, A., and Bellen, H. J. (2015) Glial lipid droplets and ROS induced by mitochondrial defects promote neurodegeneration. *Cell* **160,** 177–190

49. Alam, M. T., Manjeri, G. R., Rodenburg, R. J., Smeitink, J. A., Notebaart, R. A., Huynen, M., Willems, P. H., and Koopman, W. J. (2015) Skeletal muscle mitochondria of NDUFS4−/− mice display normal maximal pyruvate oxidation and ATP production. *Biochim. Biophys. Acta* **1847,** 526–533

50. Angelaki, D. E., and Cullen, K. E. (2008) Vestibular system: The many facets of a multimodal sense. *Annu. Rev. Neurosci.* **31,** 125–150

51. Yates, B. J., Billig, I., Cotter, L. A., Mori, R. L., and Card, J. P. (2002) Role of the vestibular system in regulating respiratory muscle activity during movement. *Clin. Exp. Pharmacol. Physiol.* **29,** 112–117

52. De Zeeuw, C. I., Simpson, J. I., Hoogenraad, C. C., Galjart, N., Koekkoek, S. K., and Ruigrok, T. J. (1998) Microcircuitry and function of the inferior olive. *Trends Neurosci.* **21,** 391–400

53. Braak, H., Rüb, U., Sandmann-Keil, D., Gai, W. P., de Vos, R. A., Jansen Steur, E. N., Arai, K., and Braak, E. (2000) Parkinson's disease: affection of brain stem nuclei controlling premotor and motor neurons of the somatomotor system. *Acta Neuropathol.* **99,** 489–495

54. Jones, B. E., and Yang, T. Z. (1985) The efferent projections from the reticular formation and the locus coeruleus studied by anterograde and retrograde axonal transport in the rat. *J. Comp. Neurol.* **242,** 56–92

55. Matsuyama, K., Ohta, Y., and Shigemi, S. (1988) Ascending and descending projections of the nucleus reticularis gigantocellularis in the cat demonstrated by the anterograde neural tracer, Phaseolus vulgaris leucoagglutinin (PHA-L). *Brain Res.* **460,** 124–141

56. Choi, W. S., Kruse, S. E., Palmiter, R. D., and Xia, Z. (2008) Mitochondrial complex I inhibition is not required for dopaminergic neuron death induced by rotenone, MPP+, or paraquat. *Proc. Natl. Acad. Sci. U.S.A.* **105,** 15136–15141

57. Valsecchi, F., Monge, C., Forkink, M., de Groof, A.J., Benard, G., Rossignol, R., Swarts, H. G., van Emst-de Vries, S. E., Rodenburg, R. J., Calvaruso, M. A., Nijtmans, L. G., Heeman, B., Roestenberg, P., Wieringa, B., Smeitink, J. A., Koopman, W. J., and Willems, P. H. (2012) Metabolic consequences of NDUFS4 gene deletion in immortalized mouse embryonic fibroblasts. *Biochim. Biophys. Acta* **1817,** 1925–1936

58. Valsecchi, F., Grefte, S., Roestenberg, P., Joosten-Wagenaars, J., Smeitink, J. A., Willems, P. H., and Koopman, W. J. (2013) Primary fibroblasts of NDUFS4−/− mice display increased ROS levels and aberrant mitochondrial morphology. *Mitochondrion* **13,** 436–443

59. Karkucinska-Wieckowska, A., Lebiedzinska, M., Jurkiewicz, E., Pajdowska, M., Trubicka, J., Szymanska-Debinska, T., Suski, J., Pinton, P., Duszyn-

ski, J., Pronicki, M., Wieckowski, M. R., and Pronicka, E. (2011) Increased reactive oxygen species (ROS) production and low catalase level in fibroblasts of a girl with MEGDEL association (Leigh syndrome, deafness, 3-methylglutaconic aciduria). *Folia Neuropathol.* **49,** 56–63

60. Mast, J. D., Tomalty, K. M., Vogel, H., and Clandinin, T. R. (2008) Reactive oxygen species act remotely to cause synapse loss in a Drosophila model of developmental mitochondrial encephalopathy. *Development* **135,** 2669–2679

61. Papa, S., Petruzzella, V., Scacco, S., Sardanelli, A. M., Iuso, A., Panelli, D., Vitale, R., Trentadue, R., De Rasmo, D., Capitanio, N., Piccoli, C,, Papa, F., Scivetti, M., Bertini, E., Rizza, T,, and De Michele, G. (2009) Pathogenetic mechanisms in hereditary dysfunctions of complex I of the respiratory chain in neurological diseases. *Biochim. Biophys. Acta* 1787, 502–517

62. Lin, C. S., Sharpley, M. S., Fan, W., Waymire, K. G., Sadun, A. A., Carelli, V., Ross-Cisneros, F. N., Baciu, P., Sung, E., McManus, M. J., Pan, B. X., Gil, D. W., Macgregor, G. R., Wallace, D. C. (2012) Mouse mtDNA muta nt model of Leber hereditary optic neuropathy. *Proc. Natl. Acad. Sci. U.S.A.* **109,** 20065–20070

63. Choi, W. S., Palmiter, R. D., and Xia, Z. (2011) Loss of mitochondrial complex I activity potentiates dopamine neuron death induced by microtubule dysfunction in a Parkinson's disease model. *J. Cell Biol.* **192,** 873–882

64. Britto, P. J., Knipling, L., and Wolff, J. (2002) The local electrostatic environment determines cysteine reactivity of tubulin. *J. Biol. Chem.* **277,** 29018–29027

65. Xiao, Z., Mi, L., Chung, F. L., and Veenstra, T. D. (2012) Proteomic analysis of covalent modifications of tubulins by isothiocyanates. *J. Nutr.* **142,** 1377S-1381S

66. Ozols, J., and Caron, J. M. (1997) Posttranslational modification of tubulin by palmitoylation: II. Identification of sites of palmitoylation. *Mol. Biol. Cell* **8,** 637–645

67. Zhao, Z., Hou, J., Xie, Z., Deng, J., Wang, X., Chen, D., Yang, F., and Gong, W. (2010) Acyl-biotinyl exchange chemistry and mass spectrometry-based analysis of palmitoylation sites of in vitro palmitoylated rat brain tubulin. *Protein J.* **29,** 531–537

68. Natale, M., Bonino, D., Consoli, P., Alberio, T., Ravid, R. G., Fasano, M., and Bucci, E. M. (2010) A meta-analysis of two-dimensional electrophoresis pattern of the Parkinson's disease-related protein DJ-1. *Bioinformatics* **26,** 946–952

69. Colombini, M. VDAC: the channel at the interface between mitochondria and the cytosol. *Mol, Cell. Biochem.* 256- 257:107–115, 2004

70. Lemasters, J. J., and Holmuhamedov, E. (2006) Voltage-dependent anion channel (VDAC) as mitochondrial governator–thinking outside the box. *Biochim. Biophys. Acta* **1762,** 181–190

71. Rostovtseva, T., and Colombini, M. (1996) ATP flux is controlled by a

voltage-gated channel from the mitochondrial outer membrane. *J. Biol. Chem.* **271,** 28006–28008

72. Rostovtseva, T., and Colombini, M. (1997) VDAC channels mediate and gate the flow of ATP: implications for the regulation of mitochondrial function. *Biophys. J.* **72,** 1954–1962

73. Rostovtseva T. K., Komarov, A., Bezrukov, S. M., and Colombini, M. (2002) VDAC channels differentiate between natural metabolites and synthetic molecules. *J. Membr. Biol.* **187,** 147–156

74. Cheng, E. H., Sheiko, T. V., Fisher, J. K., Craigen, W. J., and Korsmeyer, S. J. (2003) VDAC2 inhibits BAK activation and mitochondrial apoptosis. *Science* **301,** 513–517

75. Cerqueira Cesar, M., and Wilson, J. E. (2004) All three isoforms of the voltage-dependent anion channel (VDAC1, VDAC2, and VDAC3) are present in mitochondria from bovine, rabbit, and rat brain. *Arch. Biochem. Biophys.* **422,** 191–196

76. Maurya, S. R., and Mahalakshmi, R. (2013) Modulation of human mitochondrial voltage-dependent anion channel 2 (hVDAC-2) structural stability by cysteine-assisted barrel-lipid interactions. *J. Biol. Chem.* **288,** 25584–25592

77. Aram, L., Geula, S., Arbel, N., and Shoshan-Barmatz, V. (2010) VDAC1 cysteine residues: topology and function in channel activity and apoptosis. *Biochem. J.* **427,** 445–454

78. Tewari, S. G., Zhou, Y., Otto, B. J., Dash, R. K., Kwok, W. M., and Beard, D. A. (2015) Markov chain Monte Carlo based analysis of post-translationally modified VDAC gating kinetics. *Front. Physiol.* 2015 Jan 13;5: 513. doi: 10.3389/fphys.2014.00513

79. Doring, C., and Colombini, M. (1985) Voltage dependence and ion selectivity of the mitochondrial channel, VDAC, are modified by succinic anhydride. *J. Membr. Biol.* **83,** 81–86

80. Das, S., Wong, R., Rajapakse, N., Murphy, E., and Steenbergen, C. (2008) Glycogen synthase kinase 3 inhibition slows mitochondrial adenine nucleotide transport and regulates voltage-dependent anion channel phosphorylation. *Circ. Res.* **103,** 983–991

81. Gupta, R., and Ghosh, S. (2015) Phosphorylation of voltage-dependent anion channel by c-Jun N-terminal Kinase-3 leads to closure of the channel. *Biochem. Biophys. Res. Commun.* **459,** 100–106

82. Rostovtseva, T. K., and Bezrukov, S. M. (2012) VDAC inhibition by tubulin and its physiological implications. *Biochim. Biophys. Acta* **1818,** 1526–1535

83. Lazarou, M., Stojanovski, D., Frazier, A. E., Kotevski, A., Dewson, G., Craigen, W. J., Kluck, R. M., Vaux, D. L., and Ryan, M. T. (2010) Inhibition of Bak activation by VDAC2 is dependent on the Bak transmembrane anchor. *J. Biol. Chem.* **285,** 36876–36883

84. Maurya, S. R., and Mahalakshmi, R., (2014) Influence of protein-micelle ratios and cysteine residues on the kinetic stability and unfolding rates of human mitochondrial VDAC-2. PLoS ONE 9(1):e87701